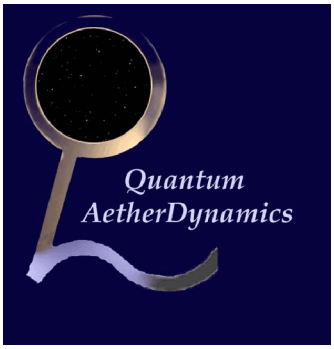

Quantum AetherDynamics Institute (QADI)

Alma, Illinois, USA

Electron $g-2$ from the APM phtn at Aether-Unit Resolution

Structural Model, QMU Magnetic Response, and Comparison with Measurement

David W. Thomson III
Quantum AetherDynamics Institute (QADI), Alma, Illinois, USA
ORCID: 0000-0002-5830-5427

Version 1.10.2 – October 19, 2026

This article is published by the Quantum AetherDynamics Institute (QADI).

It develops the Aether Physics Model (APM)

Abstract

This paper calculates the leading electron magnetic response of the Aether Physics Model (APM) from an occupied-Ligamen structural model and Quantum Measurement Units (QMU). The electron occupies a fixed-electrostatic-polarity, zero-winding boundary sector of the five-dimensional dynamical closure space within the six-dimensional chronogeometry. A port-spin construction and reciprocal propagation pair give explicit boundary matrices and a mass shell under stated minimal transport closures; a same-geometry counterfamily identifies the choices not fixed by geometry. Minimal coupling gives $g_0 = 2$. QMU charge/action closure and Coulomb-source normalization fix the dimensionless interaction coordinate

$$\alpha_e = \frac{e^2}{8\pi e_{e\,\max}^2} = \frac{g_{\mathrm{em}}^2}{4\pi},$$

without fitting the electron magnetic anomaly.

The aligned one-handoff phtn operator $\mathcal{D}_{\mathrm{phtn}} = -\Delta_u\Delta_v$, with symbol $2(\cos\Omega - \cos K)$, factors into a local characteristic operator and a normalized cell registration:

$$\mathcal{D}_{\mathrm{phtn}} = \mathcal{A}_{\mathrm{cell}}\mathcal{D}_0, \qquad \mathcal{C}_{\mathrm{cell}} = \operatorname{sinc}\frac{K-\Omega}{2}\operatorname{sinc}\frac{K+\Omega}{2}.$$

Within the stated minimal continuum completion, the square-root registered action supplies conjugate release and recapture endpoints. Their factors cancel the cell multiplier in a complete internal exchange. The resulting leading magnetic-response integral gives

$$\delta_e^{(1)} = \frac{|g_e|^{(1)} - 2}{2} = \frac{\alpha_e}{2\pi} = \frac{e^2}{16\pi^2 e_{e\,\max}^2}.$$

Thus a simple QMU charge ratio is obtained from the proposed dynamics rather than identified with the anomaly solely by a force-ratio analogy.

Using the rubidium atom-recoil determination of the coupling, independently of the electron anomaly, the leading prediction is $\delta_e^{(1)} = 0.00116140973185$. The cited Penning-trap result is $0.00115965218059(13)$. The predicted-minus-measured difference is $+1.75755126 \times 10^{-6}$, or approximately 0.151558% of the measured anomaly. A cesium recoil input gives essentially the same leading residual. No fitted correction or imported higher-order coefficients are included in the APM prediction.

The scientific conclusion is a calculated leading APM response close to the observed anomaly, with a resolved structural and cell-registration calculation under explicit boundary assumptions. The remaining numerical difference is an open physical question. The paper does not claim reproduction at experimental precision, an all-orders equivalence, or a demonstrated apparatus explanation for the residual.

Keywords: electron $g-2$; anomalous magnetic moment; Aether Physics Model; Quantum Measurement Units; APM phtn; occupied-Ligamen action; characteristic-cell registration; phtn-to-Maxwell reduction; QMU–gauge coupling matching; Ward–Takahashi identity; Pauli form factor; six-dimensional chronogeometry; five-dimensional dynamical closure; Ligamen Circulatus

Version 1.10 Revision Note

This revision retains the leading APM prediction and its open empirical residual. Section 5 now constructs the boundary matrices from the orthogonal port triad, temporal complex convention, occupied spin lift, and a reciprocal propagation pair. A classification of minimal Hermitian transport generators derives the mass shell after the common-speed and native-loading conditions are specified.

A same-geometry counterfamily proves that those remaining transport choices cannot be inferred from static geometry alone. The spinorial occupied-state map is also kept explicit as an open microscopic problem.

Section 15 adds the empirical remainder's sign and scale in units of $(\alpha_e/\pi)^2$, without identifying it with a second-order mechanism. The supporting script checks the new matrix algebra, reciprocal generator, QMU dispersion, and counterfamily, and records the normalized residual. No change to the leading anomaly prediction or its coupling inputs is made.

1 Introduction

The electron magnetic moment is an unusually stringent test of any microscopic theory of charged half-spin matter. In positive-magnitude convention,

$$\delta_e \equiv \frac{|g_e| - 2}{2} = F_2(0), \tag{1}$$

where $F_2(0)$ is the zero-momentum Pauli form factor. The leading radiative contribution is conventionally

$$F_2^{(1)}(0) = \frac{\alpha}{2\pi}, \tag{2}$$

and modern Penning-trap measurements determine $g/2$ at the sub-part-per-trillion level Schwinger [1948], Fan et al. [2023].

For APM the decisive question is whether its electron structure and phtn interaction produce a definite magnetic response that can be compared with observation. Agreement with a particular theoretical ontology is not an additional requirement. A QMU rewriting alone would not answer this question; a dynamical calculation and an explicit empirical residual are needed. Earlier revisions progressively removed weaker identifications. The force ratio $F_E/F_M = \alpha_{\mathrm{QMU}}/(2\pi)$ was separated from the anomaly calculation; the QMU charge coordinate was separated from the canonical gauge coupling and then matched by theorem; compact temporal-mode conservation was derived; and the rank-six occupied projector was separated from the normalized one-electron state. One issue remained: the internal line in the actual loop was still the already-reduced boundary gauge propagator.

The characteristic-cell construction addresses that issue within the stated minimal continuum completion at Aether-unit resolution. The phtn remains the exchanged object. Its exact discrete handoff operator is combined with the characteristic-cell release and recapture factors generated by the occupied-Ligamen action. Only the complete internal history reduces to the massless boundary gauge line.

The load-bearing chain is

$$
\begin{array}{c}
A_u e_{e\,\max}^2 = hc, \quad A_u = 16\pi^2 k_C \\
\downarrow \\
\alpha_{\mathrm{QMU}} = \dfrac{k_C e^2}{\hbar c} \\
\downarrow \\
U(1)_{es} \text{ source matching and canonical normalization} \\
\downarrow \\
\alpha_{\mathrm{gauge}} = \dfrac{g_{\mathrm{em}}^2}{4\pi} = \alpha_{\mathrm{QMU}} \equiv \alpha_e \\
\downarrow \\
\text{occupied five-dimensional charged-spinor boundary operator} \\
\downarrow \\
\text{exact APM phtn operator } \mathcal{D}_{\mathrm{phtn}} = -\Delta_u \Delta_v, \quad \Omega^2 = K^2 \\
\downarrow \\
\text{locality + reciprocity + gaplessness + minimal second order} \\
\downarrow \\
\mathcal{D}_0 = \partial_T^2 - \partial_X^2 = -\partial_u \partial_v \\
\downarrow \\
\mathcal{D}_{\mathrm{phtn}} = \mathcal{A}_{\mathrm{cell}} \mathcal{D}_0, \quad \mathcal{A} = \mathcal{B}_{\mathrm{cell}} a \\
\downarrow \\
\text{two handed phtn states} \iff \text{two transverse polarizations} \\
\downarrow \\
B_{\mathrm{rec}}\, \mathcal{D}_{\mathrm{phtn}}^{-1}\, B_{\mathrm{rel}} = \mathcal{D}_0^{-1} \\
\downarrow \\
\text{occupied zero-winding phtn vertex history} \\
\downarrow \\
F_2^{(1)}(0) = \dfrac{\alpha_e}{2\pi}.
\end{array}
\tag{3}
$$

The independent QMU force calculation still gives $F_E/F_M = \alpha_{\mathrm{QMU}}/(2\pi)$ and is not used to evaluate the loop. Its equality with the one-loop Pauli response occurs only after the separately derived coupling theorem.

The scope of the calculation is explicit. Prior APM/QMU work supplies the Aether Unit, the one-moment phtn handoff, the exact aligned phtn dispersion, scanning-worldsheet and receiver actions, the electrostatic $U(1)_{es}$ sector, charge/action closure, the occupied projector, and the half-angle temporal state. The boundary algebra and mass shell are reconstructed below from the port spin frame and a reciprocal transport pair. Memoryless unitary evolution, the minimal derivative class, the occupied spin lift, and the common-speed/loading closure remain explicit inputs. This paper derives the minimal local massless boundary operator from the exact phtn dispersion, the transverse vector lift from the two handed phtn states, the characteristic-cell registration, the phtn-to-Maxwell Green reduction, gauge covariance of the registered action, the associated Ward identity, and the minimal tree and one-loop magnetic response. The geometric reconstruction identifies both the consequences and the remaining transport inputs of the present structural model. The residual beyond its calculated leading response is also open; it is not assigned in advance to a particular theory or microscopic mechanism.

2 What Electron $g-2$ Measures

2.1 From $g-2$ to a form factor

For an on-shell electron interacting with an external electromagnetic field, the renormalized vertex can be written

$$\Gamma^{\mu}(q) = F_1(q^2)\gamma^{\mu} + F_2(q^2)\frac{i\sigma^{\mu\nu}q_{\nu}}{2m_e}. \tag{4}$$

Charge normalization gives $F_1(0) = 1$. The Pauli form factor at zero momentum transfer is the anomalous magnetic moment,

$$\boxed{\delta_e = F_2(0).} \tag{5}$$

Thus $g-2$ is not an arbitrary correction attached to the electron. It is the zero-momentum magnetic susceptibility encoded in the quantum electromagnetic vertex.

At leading radiative order,

$$F_2^{(1)}(0) = \frac{\alpha}{2\pi}. \tag{6}$$

2.2 The measured response and the prediction target

For the idealized weak-field response, the spin and cyclotron frequencies satisfy

$$\frac{|g_e|}{2} = \frac{\nu_s}{\nu_c}, \qquad \delta_e = \frac{\nu_s - \nu_c}{\nu_c} = \frac{\nu_a}{\nu_c}. \tag{7}$$

In a real Penning trap the measured motional frequencies require trap and cavity corrections before this free-response ratio is inferred Fan et al. [2023]. Equation (7) identifies the observable to which the APM response must connect. This paper calculates the homogeneous, weak-field electron response; it does not calculate the complete trap environment.

The prediction is evaluated at the first nonzero interaction order. Writing

$$\delta_e^{\text{phys}} = \delta_e^{(1)} + \Delta_e, \qquad \delta_e^{(1)} = \frac{\alpha_e}{2\pi}, \tag{8}$$

defines Δ_e as the response not determined by this leading calculation. The measured residual is a diagnostic of that incompleteness, not a derived correction. No controlled theoretical error bound on Δ_e is established here.

2.3 Independent coupling input

The QMU expression $\alpha_e = e^2/(8\pi e^2_{e\,\max})$ specifies the interaction coordinate. Its absolute numerical value is an empirical input in this paper; it is not predicted from the structural model. For the numerical test we use atom-recoil determinations Morel et al. [2020], Parker et al. [2018], rather than infer α_e from the electron anomaly being tested. Those inputs are independent of that anomaly measurement, although their extraction retains its own atomic-metrology assumptions. No claim of completely theory-free metrology is made. The dimensionless QMU expression remains the same for either recoil input.

The familiar higher-order QED expansion is an external comparison framework. Its coefficients are not inserted into the APM result or used to remove the residual in this paper. Additional APM response contributions must be calculated from specified occupied-state dynamics before they can count as predictions.

3 APM Charge Structure and the QMU Coupling Coordinate

3.1 Two physical charge structures

APM distinguishes ordinary electrostatic charge from distributed magnetic square-charge. For a species x, occupied LC angular momentum is

$$h_x = m_x \lambda_C^2 F_q, \tag{9}$$

and Aether conductance generates

$$\boxed{e_{x\,\max}^2 = h_x\,\mathrm{cond.}} \tag{10}$$

For the electron, $e_{e\,\max}^2 = h_e\mathrm{cond}$. Define the QMU fine-structure coordinate by the ratio of the two charge registrations,

$$\boxed{\alpha_{\mathrm{QMU}} \equiv \frac{e^2}{8\pi e_{e\,\max}^2}.} \tag{11}$$

Equivalently,

$$e^2 = 8\pi \alpha_{\mathrm{QMU}} e_{e\,\max}^2. \tag{12}$$

Equation (11) is a QMU charge-ledger definition. At this stage it is deliberately not identified with a canonically normalized quantum-field coupling Thomson III [2025b, 2026h].

3.2 Commensurate electron force channels

At the electron quantum scale,

$$F_E = k_C \frac{e^2}{\lambda_C^2}, \tag{13}$$

$$F_M = A_u \frac{e_{e\,\max}^2}{\lambda_C^2}. \tag{14}$$

With $A_u = 16\pi^2 k_C$,

$$\boxed{\varepsilon_e \equiv \frac{F_E}{F_M} = \frac{k_C e^2}{A_u e_{e\,\max}^2} = \frac{\alpha_{\mathrm{QMU}}}{2\pi}.} \tag{15}$$

The magnetic channel also reduces to the native QMU electron force standard $F_M = m_e \lambda_C F_q^2$ Thomson III [2026h].

3.3 Why the force ratio is not the anomaly derivation

Equation (15) is established before an electron vertex is calculated. It therefore identifies an APM/QMU interaction coordinate, but it does not prove that the Pauli form factor equals that ratio. No equation of the form $\delta F_M = F_E$ or $\Delta h_e = F_E \lambda_C t_q$ is used in this calculation. The magnetic response is calculated from the boundary vertex in Sec. 11. Before that comparison can even be stated consistently, however, the QMU charge coordinate α_{QMU} must be matched to the canonical gauge coupling. That is the purpose of the next section.

4 Canonical Electrostatic Normalization and the QMU–Gauge Matching Theorem

4.1 The QMU action scale

Two established QMU closures are

$$\boxed{A_u e_{e\,\max}^2 = \mathrm{phtn} = hc,} \tag{16}$$

and

$$\boxed{A_u = 16\pi^2 k_C.} \tag{17}$$

The first identifies the distributed electron magnetic square-charge with the QMU photon/action scale; the second is the Aether-to-electrostatic modulus ratio Thomson III [2026h,e, 2025d]. Combining them and using $h = 2\pi\hbar$ gives

$$16\pi^2 k_C e_{e\,\max}^2 = 2\pi\hbar c, \tag{18}$$

so

$$\boxed{\hbar c = 8\pi k_C e_{e\,\max}^2.} \tag{19}$$

Equation (19) immediately converts the QMU charge coordinate into

$$\boxed{\alpha_{\mathrm{QMU}} = \frac{k_C e^2}{\hbar c}.} \tag{20}$$

No boundary gauge coupling has been used in this result.

4.2 Source normalization from the APM Coulomb law

The electrostatic part of the prior dual-$U(1)$ APM field theory has kinetic normalization $1/(4k_C)$. In the local topologically trivial electrostatic sector, write its source-coupled action density as

$$\mathcal{L}_{es} = -\frac{1}{4k_C} F_{es}^{\mu\nu} F_{\mu\nu}^{es} - Q_e^{(es)} j^\mu A_\mu^{es}, \tag{21}$$

where j^μ is a unit-number current and $Q_e^{(es)}$ is the signed source coefficient in this QMU field normalization. The overall sign of the kinetic term depends on metric convention and does not affect the normalization argument. Variation gives

$$\partial_\nu F_{es}^{\nu\mu} = k_C Q_e^{(es)} j^\mu. \tag{22}$$

For a static point source, $j^0 = \delta^3(\mathbf{r})$, spherical Green-function normalization gives

$$E_{es}(r) = \frac{k_C Q_e^{(es)}}{4\pi r^2}. \tag{23}$$

A second identical source therefore experiences

$$F_{es}(r) = \frac{k_C (Q_e^{(es)})^2}{4\pi r^2}. \tag{24}$$

The independently established APM electrostatic force law is

$$F_E(r) = \frac{k_C e^2}{r^2}. \tag{25}$$

Matching Eqs. (24) and (25) fixes the source normalization rather than assuming it:

$$\boxed{(Q_e^{(es)})^2 = 4\pi e^2.} \tag{26}$$

Thus e is the QMU electrostatic charge magnitude appearing in the Coulomb ledger, whereas $Q_e^{(es)}$ is the coefficient multiplying a unit current in the $1/(4k_C)$ gauge-field normalization.

4.3 Canonical field normalization

Define the canonically normalized boundary potential by

$$A_\mu^{es} = \sqrt{k_C \hbar c}\, \mathcal{A}_\mu, \qquad F_{\mu\nu}^{es} = \sqrt{k_C \hbar c}\, \mathcal{F}_{\mu\nu}. \tag{27}$$

Using $x^0 = ct$, the dimensionless action is written as $S/\hbar = \int d^4x\, \mathcal{L}/(\hbar c)$. With this convention, Eq. (21) becomes

$$\frac{\mathcal{L}_{es}}{\hbar c} = -\frac{1}{4}\mathcal{F}_{\mu\nu}\mathcal{F}^{\mu\nu} - q_e j^\mu \mathcal{A}_\mu, \tag{28}$$

with dimensionless signed canonical charge

$$q_e = Q_e^{(es)} \sqrt{\frac{k_C}{\hbar c}}, \qquad g_{\mathrm{em}} \equiv |q_e|. \tag{29}$$

Define the gauge coupling coordinate

$$\boxed{\alpha_{\mathrm{gauge}} \equiv \frac{g_{\mathrm{em}}^2}{4\pi}.} \tag{30}$$

Using Eqs. (26) and (29),

$$\alpha_{\mathrm{gauge}} = \frac{(Q_e^{(es)})^2 k_C}{4\pi\hbar c} = \frac{k_C e^2}{\hbar c}. \tag{31}$$

Theorem 4.1 (QMU–gauge coupling matching)**.** *For the minimal local electrostatic eigenmode with kinetic normalization $1/(4k_C)$, QMU photon/action closure, and the APM Coulomb force law,*

$$\boxed{\alpha_{\mathrm{gauge}} = \alpha_{\mathrm{QMU}}.} \tag{32}$$

Therefore the common matched electron coupling may be denoted

$$\boxed{\alpha_e \equiv \alpha_{\mathrm{QMU}} = \alpha_{\mathrm{gauge}} = \frac{k_C e^2}{\hbar c} = \frac{e^2}{8\pi e_{e\,\max}^2}.} \tag{33}$$

Proof. Equation (19) gives $\alpha_{\mathrm{QMU}} = k_C e^2/(\hbar c)$. The Coulomb-law source match gives $(Q_e^{(es)})^2 = 4\pi e^2$. Canonical normalization then gives $g_{\mathrm{em}}^2 = (Q_e^{(es)})^2 k_C/(\hbar c)$, hence $\alpha_{\mathrm{gauge}} = g_{\mathrm{em}}^2/(4\pi) = k_C e^2/(\hbar c) = \alpha_{\mathrm{QMU}}$. □

4.4 Scope of the matching in the dual-$U(1)$ theory

The prior APM gauge theory also contains a metric-independent topological mixing term between the electrostatic and magnetic $U(1)$ sectors Thomson III [2025c]. In the perturbative topologically trivial sector used for the electron boundary calculation, with no monopole insertion or nontrivial global flux changing the local electrostatic eigenmode, this term does not alter the local Coulomb Green-function normalization used above. A nontrivial topological sector or induced electric–magnetic shear would require diagonalizing the full coupling matrix before applying the matching theorem and could generate an additional testable correction. This calculation makes no such correction part of the minimal electron $g-2$ calculation.

5 Geometric Boundary Propagation and the Tree-Level Electron

5.1 The APM half-angle lift

APM half-spin transport carries an intrinsic phase coordinate

$$\boxed{\zeta_h(\Phi) = \exp\left(\frac{ih\Phi}{2}\right), \qquad h = \pm 1.} \tag{34}$$

It obeys

$$\zeta_h(\Phi + 2\pi) = -\zeta_h(\Phi), \qquad \zeta_h(\Phi + 4\pi) = \zeta_h(\Phi). \tag{35}$$

Thus the intrinsic occupied half-spin state distinguishes a 2π branch change from 4π closure Thomson III [2026e]. This supplies the APM double-cover behavior required of a spin-$\frac{1}{2}$ boundary state; it does not by itself determine a magnetic anomaly. This paper treats Eq. (34) as prior APM kinematics. It does not claim to rederive the half-angle phase from the loxodrome or occupied projector in this paper.

5.2 Geometric data and the boundary reconstruction problem

The six-port fabric supplies three orthonormal interface directions and their antipodes,

$$\mathcal{N} = \{\pm\mathbf{e}_1, \pm\mathbf{e}_2, \pm\mathbf{e}_3\}, \qquad \mathbf{e}_i \cdot \mathbf{e}_j = \delta_{ij}, \qquad \sum_{\mathbf{n}\in\mathcal{N}} n_i n_j = 2\delta_{ij}. \tag{36}$$

The balanced temporal plane supplies an oriented complex structure $J_T^2 = -I$; the occupied half-angle lift supplies the phase sign to be represented at the boundary. The inherited one-handoff scales are λ_C and $t_q = F_q^{-1}$ Thomson III [2026a,b]. These are the geometric ingredients used below. The six-port phtn update is unitary in the prior transport construction; extending a corresponding local norm-preserving law to the occupied electron is an additional transport closure, not a conclusion from port positions alone.

The task is to construct the boundary matrices from these ingredients and then derive the mass shell from the transport generator. The derivation does not start by requiring a gamma matrix to square to an already assumed relativistic dispersion. Its scope is a minimal homogeneous, reciprocal boundary law. The final subsection proves why the geometric data alone cannot select that law uniquely.

5.3 From the orthogonal port triad to a two-component spin frame

Introduce the Euclidean geometric product associated with the induced port metric,

$$\mathbf{e}_i\mathbf{e}_j + \mathbf{e}_j\mathbf{e}_i = 2\delta_{ij}. \tag{37}$$

This is an algebraic encoding of the spatial inner product, not a spacetime mass-shell condition. The oriented plane generators

$$L_1 = -\mathbf{e}_2\mathbf{e}_3, \quad L_2 = -\mathbf{e}_3\mathbf{e}_1, \quad L_3 = -\mathbf{e}_1\mathbf{e}_2 \tag{38}$$

obey

$$L_iL_j = -\delta_{ij} + \epsilon_{ijk}L_k. \tag{39}$$

For example, $L_1L_2 = \mathbf{e}_2\mathbf{e}_1 = -\mathbf{e}_1\mathbf{e}_2 = L_3$. Thus the port triad determines a quaternion rotation algebra.

Use the oriented temporal plane as the complex scalar convention: $i_T^2 = -1$, with i_T represented by J_T on a real temporal plane, or by a choice of complex orientation on its handed representation. It commutes with the spatial rotation algebra. Setting $\sigma_i = i_TL_i$ gives

$$\boxed{\sigma_i\sigma_j = \delta_{ij} + i_T\epsilon_{ijk}\sigma_k.} \tag{40}$$

The minimal complex module is two dimensional. In an oriented basis, writing $i_T = i$,

$$\sigma_1 = \begin{pmatrix} 0 & 1 \\ 1 & 0 \end{pmatrix}, \quad \sigma_2 = \begin{pmatrix} 0 & -i \\ i & 0 \end{pmatrix}, \quad \sigma_3 = \begin{pmatrix} 1 & 0 \\ 0 & -1 \end{pmatrix}. \tag{41}$$

The frame rotor is

$$U(\mathbf{n},\theta) = \exp\left(-\frac{i\theta}{2}\mathbf{n}\cdot\boldsymbol{\sigma}\right), \qquad U(2\pi) = -I_2, \quad U(4\pi) = I_2. \tag{42}$$

The occupied boundary construction identifies the prior half-angle transport with this spatial spin lift. That identification remains part of the occupied-state closure: temporal phase periodicity or the metric alone does not force matter to transform in this spatial module. In particular, ordinary scalar amplitudes on six permuted port labels return to themselves after a 2π rotation; their port projector alone cannot produce the spinorial minus sign. The temporal complex convention does not identify temporal handedness with spatial spin or remove the independent temporal fiber used later.

5.4 Local transport, first-order evolution, and the minimal amplitude pair

The six-port adjacency supplies a local spatial difference,

$$\nabla_i^{\text{cell}}\psi(\mathbf{x}) = \frac{\psi(\mathbf{x}+\lambda_C\mathbf{e}_i) - \psi(\mathbf{x}-\lambda_C\mathbf{e}_i)}{2\lambda_C} = \partial_i\psi + \frac{\lambda_C^2}{6}\partial_i^3\psi + \cdots. \tag{43}$$

Selecting the leading derivative is a continuum transport approximation. Finite adjacency supplies a local difference rule; it does not make the logarithm of every discrete update an exactly local differential operator.

For differentiable, memoryless unitary boundary evolution, write

$$U(\Delta t) = I - \frac{i\Delta t}{\hbar} H + o(\Delta t). \tag{44}$$

Unitarity gives $H^\dagger = H$, and composition gives $i\hbar\partial_t\psi = H\psi$. First-order time evolution therefore follows from this transport closure. The factor $\hbar = h/(2\pi)$ only converts the native action h into radian-phase coordinates. Differentiability, memoryless composition, and the lowest spatial derivative are retained dynamical choices; a static cell metric does not prove them.

For a two-component spin frame with no preferred spatial vector, the linear momentum term is proportional to $\boldsymbol{\sigma}\cdot\mathbf{p}$. To represent the reciprocal port inversion by a linear unitary parity operation at the same electrostatic polarity, a second propagation amplitude is needed. No 2×2 unitary can reverse all three σ_i: applying such a reversal to $\sigma_1\sigma_2 = i\sigma_3$ would give $i\sigma_3 = -i\sigma_3$. Use the minimal pair

$$\psi = \begin{pmatrix}\psi_+\\ \psi_-\end{pmatrix}, \qquad \psi_\pm \in \mathbb{C}^2, \qquad \mathcal{P} = \varrho_1 \otimes I_2, \tag{45}$$

where ϱ_i are Pauli matrices acting on the propagation pair. These amplitudes are neither two electrons nor the two electrostatic carrier spheres. They are boundary components at fixed electrostatic polarity; they are not a relabeling of the separate compact temporal-handed fiber.

This construction specifies an admissible minimal boundary module. It does not derive an intertwining map from the rank-six occupied port subspace onto that module. Such a map and its occupied dynamics remain to be supplied by a microscopic LC action. A dimension count alone would not establish the required transformation law.

5.5 Reciprocity fixes the form of the minimal transport generator

At linear derivative order, equivalent-port sign reversals exclude off-diagonal directional couplings and equivalent-axis permutations equate the three diagonal coefficients. Thus the second-moment isotropy in Eq. (36), spin-frame covariance, and the absence of another preferred vector give the most general homogeneous Hermitian generator on this minimal module as

$$H(\mathbf{p}) = M\otimes I_2 + A\otimes(\boldsymbol{\sigma}\cdot\mathbf{p}), \qquad M = M^\dagger, \quad A = A^\dagger. \tag{46}$$

Require the free reciprocal law $\mathcal{P}H(\mathbf{p})\mathcal{P}^{-1} = H(-\mathbf{p})$. Hence

$$[M, \varrho_1] = 0, \qquad \{A, \varrho_1\} = 0, \tag{47}$$

and therefore

$$M = E_c I_2 + \mathcal{M}\varrho_1, \qquad A = v_2\varrho_2 + v_3\varrho_3, \tag{48}$$

with real coefficients. A pair-basis rotation around ϱ_1 takes A to $v\varrho_3$, where $v = \sqrt{v_2^2 + v_3^2}$. Remove the common phase center E_c and choose the rest orientation so $\mathcal{M} > 0$. Then

$$\boxed{H_v(\mathbf{p}) = v\,\varrho_3\otimes(\boldsymbol{\sigma}\cdot\mathbf{p}) + \mathcal{M}\varrho_1\otimes I_2.} \tag{49}$$

Reciprocity, Hermiticity, and the minimal paired spin module have fixed the matrix structure. Neither the value of v nor the rest loading $\mathcal{M}$ follows from that algebra alone.

For the electron model tested here, use the common Aether characteristic speed and the native electron loading,

$$v = c = \lambda_C F_q, \qquad \mathcal{M} = E_q \equiv m_e \,\mathrm{temp} = m_e \lambda_C^2 F_q^2 = h F_q. \tag{50}$$

Equality of the electron boundary characteristic speed to the phtn handoff speed is the common-speed transport closure; a maximum-speed bound alone would give only $v \le c$. The electron mass remains a base empirical input. Identifying the rest loading with E_q is the native loading convention of this model, not an independent prediction of m_e.

Ledger One expresses the same common-speed closure as $v^2 = A_u \,\mathrm{curl} = \mathrm{temp}$, with rest loading $E_q = m_e A_u \,\mathrm{curl}$. This connects the boundary coefficients directly to the native organizing and matter-loading units without fixing an additional anomaly parameter.

5.6 Derived mass shell, four-dimensional matrices, and QMU propagation law

Define

$$\mathsf{a}_i = \varrho_3 \otimes \sigma_i, \qquad \mathsf{b} = \varrho_1 \otimes I_2. \tag{51}$$

Their products, already fixed by the geometric rotation algebra and reciprocal pair, give

$$\{\mathsf{a}_i, \mathsf{a}_j\} = 2\delta_{ij} I_4, \qquad \{\mathsf{a}_i, \mathsf{b}\} = 0, \qquad \mathsf{b}^2 = I_4. \tag{52}$$

Consequently the chosen generator satisfies

$$H = c\,\mathbf{a}\cdot\mathbf{p} + E_q \mathsf{b}, \qquad H^2 = (c^2\mathbf{p}^2 + E_q^2) I_4. \tag{53}$$

Thus the free boundary mass shell is a consequence,

$$\boxed{E^2 = c^2\mathbf{p}^2 + m_e^2 c^4, \qquad p_\mu p^\mu = m_e^2 \quad (\hbar = c = 1),} \tag{54}$$

rather than the initial matrix-factorization requirement. Explicit spacetime matrices are

$$\boxed{\gamma^0 = \mathsf{b} = \varrho_1 \otimes I_2, \qquad \gamma^i = \mathsf{b}\mathsf{a}_i = -i\varrho_2 \otimes \sigma_i.} \tag{55}$$

They obey

$$\boxed{\{\gamma^\mu, \gamma^\nu\} = 2\eta^{\mu\nu} I_4, \qquad \eta = \mathrm{diag}(1,-1,-1,-1).} \tag{56}$$

The four-component representation is constructed, not assumed at the start. In canonical boundary coordinates the evolution becomes

$$(\gamma^\mu p_\mu - m_e)\psi_e = 0, \qquad \boxed{(i\gamma^\mu \partial_\mu - m_e)\psi_e = 0} \tag{57}$$

in natural units. This is the Dirac boundary equation Dirac [1928]; its algebra has now been obtained from a spatial spin frame and a reciprocal propagation pair under the specified transport closure.

The native QMU form needs neither a new mass scale nor a new length. With $\mathbf{X} = \mathbf{x}/\lambda_C$ and $T = F_q t$,

$$\boxed{i\partial_T \psi = [-i\mathbf{a}\cdot\nabla_X + 2\pi\mathsf{b}]\,\psi.} \tag{58}$$

For $\psi \propto e^{i(\mathbf{K}\cdot\mathbf{X}-\Omega T)}$,

$$\boxed{\Omega^2 = |\mathbf{K}|^2 + (2\pi)^2.} \tag{59}$$

The 2π is the conversion from one native action cycle to radian phase: $E_q/(\hbar F_q) = 2\pi$. This dynamical phase is distinct from the spatial 4π spin lift. A sampled one-moment return would not by itself distinguish different unwrapped phase windings; the specified loading fixes the branch used here.

The same equation gives a local continuity law,

$$\partial_t(\psi^\dagger\psi) + \nabla\cdot\mathbf{j} = 0, \qquad \mathbf{j} = c\psi^\dagger\mathbf{a}\psi, \qquad |\mathbf{j}| \le c\psi^\dagger\psi. \tag{60}$$

The bound follows because $(\mathbf{n}\cdot\mathbf{a})^2 = I_4$ for every unit $\mathbf{n}$. The constructed boundary law therefore has conserved norm and characteristic speed c. Its application over the full momenta in the magnetic-response integral remains the continuum completion stated in Sec. 10.6.

Theorem 5.1 (Geometric reconstruction with explicit transport closure)**.** *The oriented orthogonal port triad and temporal complex convention construct the Pauli algebra on the selected occupied spin lift. On its minimal reciprocal propagation pair, a homogeneous Hermitian, frame-covariant generator with at most one spatial derivative and linear unitary port parity has the form in Eq.* (49)*, up to a common phase and basis choice. With the common-speed and electron-loading conditions in Eq.* (50)*, it gives Eqs.* (55)–(60)*. The relativistic mass shell need not be imposed separately.*

5.7 What geometry alone does not determine

There is a direct underdetermination test. Keep the same port frame, temporal metric, spin lift, parity, loading E_q, and lowest-derivative form, but choose H_v in Eq. (49) with any $0 < v \le c$. Every member is Hermitian, frame covariant, parity reciprocal, and local, with the same rest gap and no propagation faster than c. Yet

$$H_v^2 = (v^2\mathbf{p}^2 + E_q^2)I_4 \tag{61}$$

gives different boundary dispersion when $v \neq c$. Thus those shared geometric data and a maximum-speed bound cannot uniquely determine the common-speed law. Allowing additional derivatives or memory enlarges the freedom further.

Likewise, a single-valued scalar port representation cannot yield the selected spin sign by an ordinary linear projection. If $R_{\mathrm{port}}(2\pi) = I$ and W intertwines it with a spinorial boundary representation $U(2\pi) = -I$, then $W = -W$, so $W = 0$. The occupied spin lift must therefore be present in the state/connection structure; it cannot be manufactured by taking a rank-six trace. The microscopic spinorial occupied map is still an open derivation.

The new result is a constructive boundary algebra and a mass shell derived within explicit minimal APM transport rules. It reduces the earlier independent mass-shell premise, but it does not establish that geometry alone selects memoryless evolution, the occupied spin module, or common-speed saturation. These are precise remaining dynamical questions, rather than assumptions concealed inside gamma-matrix factorization.

5.8 Local electrostatic gauge covariance

The coupling magnitude has already been fixed by the matching theorem, Eq. (32). The remaining role of local $U(1)_{es}$ covariance is to determine how that coupling enters the half-spin boundary field. With the canonical potential $\mathcal{A}_\mu$ and signed electron charge $q_e = -g_{\rm em}$ in the usual electron convention,

$$\psi_e \mapsto e^{-iq_e\chi(x)}\psi_e, \qquad \mathcal{A}_\mu \mapsto \mathcal{A}_\mu + \partial_\mu\chi. \tag{62}$$

The unique connection at first derivative order that makes the transformed derivative covariant is

$$\boxed{D_\mu = \partial_\mu + iq_e\mathcal{A}_\mu.} \tag{63}$$

The minimally coupled boundary operator is therefore

$$\boxed{\mathscr{D}_{\rm bdy} = i\gamma^\mu D_\mu - m_e,} \tag{64}$$

with interaction vertex

$$\boxed{V^\mu_{\rm bdy} = -iq_e\gamma^\mu.} \tag{65}$$

At fixed electrostatic polarity, temporal handedness belongs to the separate dynamical fiber rather than to the charge representation, so the minimal electrostatic generator acts as $q_e I_T$ and

$$\boxed{V^\mu_{\rm APM} = -iq_e\gamma^\mu \otimes I_T.} \tag{66}$$

Gauge covariance fixes the form of this lowest-derivative coupling; Sec. 4 fixes its normalization.

5.9 Minimal tree theory and $g_0 = 2$

Gauge covariance and Clifford factorization do not forbid every higher-dimension interaction. The minimal dimension-four boundary action is

$$\mathcal{L}^{(4)}_{\rm bdy} = \bar\psi_e(i\gamma^\mu D_\mu - m_e)\psi_e - \frac{1}{4}\mathcal{F}_{\mu\nu}\mathcal{F}^{\mu\nu}, \tag{67}$$

and contains no independent Pauli coefficient. A gauge-invariant dimension-five extension would have the form

$$\Delta\mathcal{L}_P = \frac{c_P}{M}\,\bar\psi_e\sigma^{\mu\nu}\mathcal{F}_{\mu\nu}\psi_e, \tag{68}$$

for some microscopic scale M. The minimal model therefore makes the boundary statement

$$\boxed{c_P^{\rm tree} = 0 \quad \text{in the minimal dimension-four boundary action,}} \tag{69}$$

not the stronger claim that $U(1)$ symmetry forbids Eq. (68). Within the minimal tree theory,

$$F_1^{(0)}(0) = 1, \qquad F_2^{(0)}(0) = 0. \tag{70}$$

Between on-shell spinors the Gordon identity gives

$$\bar u(p')\gamma^\mu u(p) = \bar u(p')\left[\frac{(p'+p)^\mu}{2m_e} + \frac{i\sigma^{\mu\nu}q_\nu}{2m_e}\right]u(p). \tag{71}$$

The second term is the tree spin–magnetic coupling. In the nonrelativistic limit,

$$H_B = -\frac{q_e}{m_e}\,\mathbf{S}\cdot\mathbf{B} = -g_0\frac{q_e}{2m_e}\,\mathbf{S}\cdot\mathbf{B}, \tag{72}$$

so

$$\boxed{|g_e|^{(0)} = g_0 = 2.} \tag{73}$$

Thus the baseline two follows from the minimally coupled half-spin boundary operator rather than from the QMU $8\pi/4\pi$ conversion ledger. A future microscopic occupied-Ligamen action must explain why the low-energy coefficient generated for Eq. (68) vanishes or is sufficiently suppressed; that suppression is not derived from gauge invariance alone.

6 Six-Dimensional Ontology and Five-Dimensional Dynamical Closure

6.1 Why "five-dimensional" is easy to misunderstand

In ordinary higher-dimensional field theories, an extra dimension is often pictured as an additional spatial coordinate. That is not the APM construction. The Aether-unit ontology used in this revision contains three spatial and three temporal dimensions,

$$\boxed{3S + 3T = 6D}, \qquad \mathcal{T} = T_{\mathrm{FB}} \oplus T_{\mathrm{LR}} \oplus T_E. \tag{74}$$

Their roles are distinct:

$$T_{\mathrm{FB}}: \text{ forward/backward Gforce progression,} \tag{75}$$

$$T_{\mathrm{LR}}: \text{ left/right temporal torque,} \tag{76}$$

$$T_E: \text{ static one-spin electrostatic bifurcation sector.} \tag{77}$$

The electrostatic dimension is represented as a static sector rather than an additional propagating coordinate. Write

$$\Psi_{\sigma_E}(\mathbf{x}, \Pi_T, \Pi_S), \qquad E_T\Psi_{\sigma_E} = \sigma_E\Psi_{\sigma_E}, \qquad \sigma_E = \pm 1, \qquad E_T^2 = I. \tag{78}$$

Thus the local nonconstant closure problem at fixed σ_E is

$$\boxed{3S + 2T_{\mathrm{dyn}} = 5D}. \tag{79}$$

There is no ∂_E term in the kinetic operator. The static electrostatic sector anchors polarity; forward/backward progression and temporal torque supply the two dynamical temporal coordinates. For continuity with the earlier notation, their phase coordinates are denoted Π_T and Π_S, with

$$\Phi_- = \frac{\Pi_T - \Pi_S}{2}, \qquad \Phi_+ = \frac{\Pi_T + \Pi_S}{2}. \tag{80}$$

The dynamical temporal plane has induced metric

$$G_T = \frac{{\lambda_C}^2}{8\pi^2}\begin{pmatrix} 1 & 0 \\ 0 & 1 \end{pmatrix}. \tag{81}$$

Thus T_{FB} and T_{LR} are orthogonal in the dynamical metric even though both are required to construct the temporal surface Thomson III [2026a]. Orthogonality does not mean disconnection, and neither dynamical direction is to be identified with electrostatic polarity. Reversal of T_{FB}, reversal of T_{LR}, and exchange of the T_E electrostatic sectors are three distinct operations.

6.2 The temporal plane and its built-in quarter-turn

An oriented two-dimensional plane possesses the canonical complex structure

$$J_T = \begin{pmatrix} 0 & -1 \\ 1 & 0 \end{pmatrix}, \qquad J_T^2 = -I_2. \tag{82}$$

The Aether-fabric derivation identifies the handed temporal eigenstates

$$h_+ = \frac{1}{\sqrt{2}} \begin{pmatrix} 1 \\ -i \end{pmatrix}, \qquad h_- = \frac{1}{\sqrt{2}} \begin{pmatrix} 1 \\ i \end{pmatrix}, \tag{83}$$

for which

$$J_T h_\eta = i\eta h_\eta, \qquad \eta = \pm 1. \tag{84}$$

Temporal transport through a signed twist ω is therefore

$$H(\omega) = e^{-\omega J_T}, \qquad H(\omega) h_\eta = e^{-i\eta\omega} h_\eta. \tag{85}$$

This is the mathematical reason temporal torque can distinguish handedness without assigning positive energy to one state and negative energy to the other Thomson III [2026b].

6.3 One quantum moment is not two macroscopic times

The exposed QMU quantum moment is $t_q = 1/F_q = \lambda_C/c$ with $c = F_q \lambda_C$. The APM chronogeometry contains an internal forward/backward history and a temporal-torque degree of freedom during that quantum moment. The compact internal coordinate must therefore not be interpreted as a second macroscopic clock that an external observer can independently read.

For the present construction, within either fixed electrostatic sector $\sigma_E = \pm 1$, it is useful to write

$$\mathcal{M}_5^{(\sigma_E)} = \mathcal{M}_{3+1} \times \mathbb{T}^1_T, \tag{86}$$

where $\mathbb{T}^1_T$ denotes the compact temporal-torque fiber. Equation (86) is the five-dimensional dynamical slice of the six-dimensional ontology, not a claim that the full Aether topology globally factorizes everywhere. The two electrostatic sectors are exchanged by E_T; they are not generated by forward/backward time reversal or temporal-torque reversal.

A helpful picture is this: ordinary time labels the exposed sequence of completed quantum moments; temporal torque labels internal orientation and circulation available while a moment is being completed. Internal histories may therefore differ without requiring additional externally elapsed quantum moments.

7 Deriving the Temporal Kinetic Operator

7.1 First-order factorization of the balanced temporal metric

Let

$$\partial_T \equiv \frac{\partial}{\partial \Pi_T}, \qquad \partial_S \equiv \frac{\partial}{\partial \Pi_S}. \tag{87}$$

The balanced temporal metric of Eq. (81) has a natural first-order factorization using J_T:

$$\boxed{\mathcal{K}_T = \partial_T I_2 - J_T \partial_S,} \qquad \overline{\mathcal{K}}_T = \partial_T I_2 + J_T \partial_S. \tag{88}$$

Because $J_T^2 = -I_2$ and the derivatives commute,

$$\boxed{\overline{\mathcal{K}}_T \mathcal{K}_T = \partial_T^2 + \partial_S^2.} \tag{89}$$

Thus the same complex structure that transports temporal handedness also factorizes the Laplacian of the balanced temporal plane. No arbitrary mixing coefficient is required.

Acting on the handed states,

$$\mathcal{K}_T h_\eta = (\partial_T - i\eta \partial_S) h_\eta. \tag{90}$$

Forward/backward temporal progression is common; temporal torque contributes the opposite phase to opposite handedness. This is exactly the continuum behavior suggested by the previously derived discrete transport law in Eq. (85).

7.2 Physical temporal coordinates

Introduce coordinates scaled by the quantum frequency,

$$t = \frac{\Pi_T}{2\pi F_q}, \qquad \tau = \frac{\Pi_S}{2\pi F_q}. \tag{91}$$

Then the normalized temporal generator can be written

$$D_T = \partial_t I_2 - J_T \partial_\tau. \tag{92}$$

The coordinate τ is compact and represents temporal torque. It is not assigned the status of an independently observable external time.

8 Five-Dimensional Extension of the Derived Boundary Operator

8.1 From the boundary spinor to the temporal fiber

Section 5 constructs the boundary matrices from the port spin frame and reciprocal propagation pair, derives the mass shell within explicit minimal transport closures, and couples the result through electrostatic $U(1)$ covariance. The APM chronogeometric ingredients used from prior work are the full $3S + 3T$ ontology, its $3S + 2T_{\text{dyn}}$ fixed-electrostatic-sector closure, the balanced

dynamical temporal metric, J_T, the handed temporal states, the temporal transport law, and the occupied-channel projector.

Define the Hermitian handedness operator

$$\sigma_T \equiv -iJ_T, \qquad \sigma_T^\dagger = \sigma_T, \qquad \sigma_T^2 = I_2. \tag{93}$$

The minimal five-dimensional extension is

$$\boxed{\mathscr{D}_5 = (i\gamma^\mu D_\mu - m_e) \otimes I_T - \gamma^0 \otimes \sigma_T \, (-iD_\tau).} \tag{94}$$

No fifth spatial gamma matrix is introduced. The additional term is an internal temporal-rotation generator attached to the dynamical temporal plane already present in APM. The orientation convention may be reversed by $\tau \mapsto -\tau$ without changing the closed-sector conclusions.

8.2 Compact modes

For an internal Fourier mode

$$\Psi_{n,\eta}(x,\tau) = \psi_n(x) h_\eta e^{in\tau/R_T}, \tag{95}$$

with integer n,

$$-iD_\tau \to \frac{n}{R_T}. \tag{96}$$

The kinetic operator becomes

$$\mathscr{D}_5 \Psi_{n,\eta} = \left[\not{p} - m_e + \eta\gamma^0 \frac{n}{R_T} \right] \psi_n h_\eta, \tag{97}$$

up to the orientation convention. The spectral propagator is

$$\boxed{G_5(p;\tau,\tau') = \sum_{n,\eta} P_\eta \frac{i}{\not{p} - m_e + \eta\gamma^0 n/R_T + i0} e^{in(\tau-\tau')/R_T}.} \tag{98}$$

Nonzero n sectors describe unresolved temporal-torque propagation. Persistent external electrons are identified with the closed boundary sector rather than arbitrary $n \neq 0$ modes.

9 Occupied Ligamen Closure

9.1 The rank-six occupied projector

The Aether-fabric occupancy analysis begins with a twelve-dimensional free local state space: six compatibility ports times a two-state temporal fiber. Material occupation correlates antipodal port parity B with temporal handedness. The resulting projectors are

$$\boxed{P_s = \frac{1}{2}\left(I_{12} + sB \otimes \sigma_{3,\gamma}\right), \qquad s = \pm 1,} \tag{99}$$

with

$$P_s^2 = P_s, \qquad P_s^\dagger = P_s, \qquad \operatorname{rank} P_s = 6. \tag{100}$$

The occupied electron belongs to the negative loxodromic orientation in the current species ledger Thomson III [2026g]. We therefore denote its occupied projector by P_-.

The significance of Eq. (99) is easily missed. Occupancy does not simply delete one temporal state. It correlates temporal handedness with branch parity so that one six-dimensional locked representation survives. The electron is therefore an occupied boundary condition on the full port–temporal state space.

9.2 Admissibility projector versus one-electron occupancy

The rank of P_- must not be interpreted as six independently propagating electron species. It counts the compatible components of the occupied port–temporal subspace. A single prepared electron is represented by a normalized internal state

$$\xi_e \in \operatorname{Im} P_-, \qquad \langle \xi_e | \xi_e \rangle = 1, \qquad P_- |\xi_e\rangle = |\xi_e\rangle. \tag{101}$$

Equivalently define the internal density operator

$$\boxed{\rho_e \equiv |\xi_e\rangle\langle\xi_e|,} \qquad \rho_e^2 = \rho_e, \qquad \operatorname{Tr}_{\text{int}} \rho_e = 1, \qquad P_- \rho_e = \rho_e P_- = \rho_e. \tag{102}$$

This distinction is essential for the leading occupied-electron response. P_- is an admissibility projector; ρ_e is the normalized physical occupancy of one electron. The six-dimensional admissible internal image is not, by itself, a count of six electron species. Conversely, external normalization alone does not specify the measure or weights of independent closed internal histories. Those questions are not needed for the leading vertex graph calculated here. The microscopic LC action should eventually derive the specific coherent state ξ_e rather than merely the admissible image of P_-.

9.3 Closed temporal winding

Define Π_{cl} to project onto zero net compact temporal-torque winding,

$$\Pi_{\text{cl}} : \quad n = 0. \tag{103}$$

This does not mean that the internal history was trivial. It means that after the complete internal process no unresolved temporal-fiber momentum remains in the persistent boundary state.

For $n = 0$, Eq. (98) becomes

$$G_{5,0}(p) = \frac{i}{\not{p} - m_e + i0} \otimes I_T = S_F(p) \otimes I_T. \tag{104}$$

Since the ordinary Dirac propagator acts on the spinor factor and P_- acts on the APM internal factor, they commute. Therefore

$$P_- G_{5,0} P_- = S_F \otimes P_-. \tag{105}$$

Theorem 9.1 (Occupied 5D boundary reduction)**.** *For the minimal operator in Eq. (94), an occupied electron satisfying zero net compact temporal winding has boundary propagator*

$$\boxed{\Pi_{\mathrm{cl}} P_- \mathscr{D}_5^{-1} P_- \Pi_{\mathrm{cl}} = S_F^{(4)} \otimes P_-.} \tag{106}$$

Proof. The closed-winding projector sets $n = 0$ in the spectral representation, eliminating the internal temporal-torque term from the denominator. The remaining propagator is proportional to the identity on the temporal fiber. It therefore commutes with P_-. Idempotence $P_-^2 = P_-$ then gives Eq. (106). □

The theorem supplies a precise meaning for the phrase "four-dimensional observation of a five-dimensional electron." The ordinary propagator is the closed occupied boundary image of the larger internal state space.

10 Minimal Occupied-Ligamen Action and Characteristic-Cell Registration

10.1 Resolution and dynamical variables

The phrase "complete occupied-Ligamen action" must be tied to a resolution scale. Existing APM work takes the Aether Unit as the primitive dynamical cell; it does not derive that Unit from a finer continuum. The action below includes the fields used in the present leading-response model. It does not define every interacting occupied sector or establish microscopic completeness.

Let Ψ be the occupied five-dimensional electron field, Ξ the occupied-seat state, a_μ the underlying phtn transport potential, and $\mathcal{A}_\mu$ the registered boundary connection seen by the persistent electron. The minimal action will be

$$\boxed{S_{\mathrm{OL}}^{\mathrm{min}} = S_{e,5}[\Psi, \mathcal{A}] + S_{\mathrm{seat}}[\Xi] + S_{\mathrm{phtn}}[a].} \tag{107}$$

The occupied mismatch term is inherited from the chirality-matched receiver action,

$$\boxed{S_{\mathrm{seat}}^{(q)} = t_q m_e c^2 \langle \Xi, Q_- \Xi \rangle = h \langle \Xi, Q_- \Xi \rangle, \qquad Q_- \equiv I - P_-.} \tag{108}$$

Its minimum is $P_- \Xi = \Xi$ Thomson III [2026f]. The remaining task is to determine S_{phtn} and the map from a_μ to $\mathcal{A}_\mu$ from the exact one-handoff dynamics rather than by inserting a continuum photon propagator.

10.2 One-handoff characteristic cell

Choose the dynamically aligned phtn current as the local longitudinal direction and define

$$X \equiv \frac{x_{\parallel}}{\lambda_C}, \qquad T \equiv \frac{t}{t_q}, \qquad t_q = F_q^{-1}. \tag{109}$$

The free Aether-fabric operator advances one spacing $d_A = \lambda_C$ in one quantum moment, so $d_A/t_q = c$ exactly Thomson III [2026b]. Introduce characteristic coordinates

$$\boxed{u = \frac{X+T}{2}, \qquad v = \frac{X-T}{2}.} \tag{110}$$

A unit increment in u at fixed v gives $(\Delta X, \Delta T) = (1, 1)$, while a unit increment in v at fixed u gives $(1, -1)$. The centered reciprocal one-handoff cell is

$$\mathcal{C}_0 = \left[-\frac{1}{2}, \frac{1}{2}\right]_u \times \left[-\frac{1}{2}, \frac{1}{2}\right]_v, \tag{111}$$

which becomes the characteristic diamond

$$\boxed{|X| + |T| \le 1} \tag{112}$$

in longitudinal-time coordinates. This is a causal transport cell, not the Euclidean area of the rendered Stage-11D loxodrome. The earlier scanning construction already distinguishes time-integrated physical support from visualization surfaces Thomson III [2026g].

The exact aligned phtn handoff operator inherited from the Aether-fabric dynamics is

$$\boxed{\mathcal{D}_{\mathrm{phtn}} = -\Delta_u \Delta_v,} \tag{113}$$

with centered differences

$$\Delta_u a = a\left(u + \frac{1}{2}, v\right) - a\left(u - \frac{1}{2}, v\right), \tag{114}$$

$$\Delta_v a = a\left(u, v + \frac{1}{2}\right) - a\left(u, v - \frac{1}{2}\right). \tag{115}$$

Its Fourier symbol is

$$\mathcal{D}_{\mathrm{phtn}}(\Omega, K) = 4 \sin\frac{K-\Omega}{2} \sin\frac{K+\Omega}{2} \tag{116}$$

$$= \boxed{2(\cos\Omega - \cos K)}. \tag{117}$$

This is the scalar factor of the independently derived physical phtn characteristic polynomial Thomson III [2026b].

10.3 Derivation of the local massless characteristic operator

The continuum operator used in the boundary representation need not be postulated independently. Let $\mathcal{D}_{\mathrm{bdy}}$ be the most general real, local, translation-invariant differential operator of minimal second order acting on one aligned physical phtn amplitude. Require the local operator to inherit the

reciprocal evenness of the exact free phtn branch under $K \mapsto -K$ and $\Omega \mapsto -\Omega$, and require the branch to remain gapless at $K = \Omega = 0$. Odd first-derivative terms are then forbidden by reciprocity, a mixed term $\partial_X \partial_T$ is odd under either reciprocal sign reversal, and a zeroth-order term would open a gap. Hence, up to an overall normalization,

$$\mathcal{D}_{\mathrm{bdy}} = a\,\partial_T^2 + b\,\partial_X^2. \tag{118}$$

On $e^{i(KX-\Omega T)}$ its symbol is $-a\Omega^2 - bK^2$. The independently derived exact aligned APM phtn branch satisfies

$$\Omega^2 = K^2 \tag{119}$$

throughout the principal phase interval Thomson III [2026b]. Requiring the zero set of Eq. (118) to coincide with Eq. (119) for arbitrary K gives $b = -a$. Canonical normalization fixes the irrelevant overall coefficient, so

$$\boxed{\mathcal{D}_0 = \partial_T^2 - \partial_X^2 = -\partial_u \partial_v.} \tag{120}$$

Its Fourier symbol is therefore $K^2 - \Omega^2$.

Theorem 10.1 (Minimal boundary-wave operator)**.** *At Aether-unit resolution, assume locality, translation invariance, the reciprocal evenness $K \mapsto -K$ and $\Omega \mapsto -\Omega$ inherited from the free phtn branch, gaplessness, and minimal second derivative order. Then the exact aligned APM dispersion $\Omega^2 = K^2$ uniquely fixes the local scalar boundary kinetic operator, up to overall normalization, to Eq.* (120)*.*

The qualifier "minimal second derivative order" is essential. Operators such as $F(\mathcal{D}_0)\mathcal{D}_0$ can share the same light-cone zero set while introducing additional scales or zeros. They describe nonminimal higher-derivative dynamics and are outside the minimal Aether-unit action tested here. Thus the massless characteristic operator used below is derived from the exact phtn dispersion plus the stated local boundary principles rather than inserted as an independent photon premise.

10.4 Characteristic-cell variational theorem

Let $\mathcal{R}$ be an initially unknown normalized, centered, translation-invariant convolution registration operator with a continuous Fourier multiplier, associated with one coherent Aether-cell transport amplitude. The same physical degree of freedom must have local kinetic operator $\mathcal{D}_0$ in its continuum boundary representation and $\mathcal{D}_{\mathrm{phtn}}$ in its exact one-handoff representation. Therefore

$$\boxed{\mathcal{D}_{\mathrm{phtn}} = \mathcal{R}\mathcal{D}_0.} \tag{121}$$

For each Fourier mode,

$$\widehat{\mathcal{R}}(\Omega, K) = \frac{\mathcal{D}_{\mathrm{phtn}}(\Omega, K)}{K^2 - \Omega^2} = \boxed{\mathrm{sinc}\left(\frac{K-\Omega}{2}\right)\mathrm{sinc}\left(\frac{K+\Omega}{2}\right)}. \tag{122}$$

Define this multiplier as $\mathcal{C}_{\mathrm{cell}}(\Omega, K)$.

Theorem 10.2 (Occupied-Ligamen characteristic-cell theorem)**.** *At Aether-unit resolution, assume one coherent electromagnetic transport amplitude per translated one-handoff cell, a normalized centered translation-invariant convolution registration with a continuous Fourier multiplier, the*

derived minimal boundary operator of Eq. (120), and the exact phtn operator $\mathcal{D}_{\mathrm{phtn}} = -\Delta_u\Delta_v$. *Then the registration is uniquely*

$$\boxed{\mathcal{R} = \mathcal{A}_{\mathrm{cell}},} \tag{123}$$

where

$$(\mathcal{A}_{\mathrm{cell}} f)(u,v) = \int_{-1/2}^{1/2} ds \int_{-1/2}^{1/2} dr\; f(u+s, v+r), \tag{124}$$

and

$$\boxed{\mathcal{D}_{\mathrm{phtn}} = \mathcal{A}_{\mathrm{cell}}\mathcal{D}_0.} \tag{125}$$

In (X,T) *coordinates the normalized real-space kernel is*

$$\boxed{w_{\mathrm{cell}}(X,T) = \frac{1}{2}\mathbf{1}_{\{|X|+|T|\le 1\}}.} \tag{126}$$

Proof. Equation (121) fixes the Fourier multiplier off the characteristic zero set. Continuity fixes its values on that set by extension, giving Eq. (122). Fourier inversion in (u,v) gives the unit top-hat on the centered square. Equivalently,

$$(\mathcal{A}_{\mathrm{cell}}\mathcal{D}_0 a)(u,v) = -\int_{-1/2}^{1/2} ds \int_{-1/2}^{1/2} dr\, \partial_u\partial_v a(u+s, v+r) \tag{127}$$

$$= -\Delta_u\Delta_v a = \mathcal{D}_{\mathrm{phtn}} a, \tag{128}$$

by two applications of the fundamental theorem of calculus. The Jacobian from (u,v) to (X,T) converts the square into the diamond in Eq. (126). Uniqueness follows from injectivity of the Fourier transform for translation-invariant convolution kernels. □

The sinc factor is therefore not a reconstruction filter appended after the discrete calculation. It is the unique one-cell registration compatible with the already established phtn handoff operator and the local massless characteristic operator.

10.5 Euclidean positivity and square-root registration

To construct the action cleanly, Wick rotate $\Omega = i\Omega_E$. Then

$$D_{\mathrm{phtn},E} = 2(\cosh\Omega_E - \cos K), \qquad D_{0,E} = K^2 + \Omega_E^2, \tag{129}$$

and

$$\boxed{C_E(K,\Omega_E) \equiv \frac{D_{\mathrm{phtn},E}}{D_{0,E}} = \mathrm{sinc}\frac{K+i\Omega_E}{2}\,\mathrm{sinc}\frac{K-i\Omega_E}{2} = \frac{4[\sin^2(K/2) + \sinh^2(\Omega_E/2)]}{K^2+\Omega_E^2} \ge 0.} \tag{130}$$

The continuous value at the origin is $C_E(0,0) = 1$. Away from the origin the only Euclidean zeros are the reciprocal-registration modes $\Omega_E = 0$, $K = 2\pi n$ with nonzero integer n. The nonnegative multiplier defines the positive square root below. Its inverse is used only on the regulated non-null domain specified next; removal of exact zeros alone does not make that inverse bounded.

$$\boxed{\mathcal{B}_{\mathrm{cell}} \equiv C_E^{1/2}.} \tag{131}$$

Because $\mathcal{B}_{\mathrm{cell}}$ is a scalar translation-invariant pseudodifferential operator,

$$[\mathcal{B}_{\mathrm{cell}}, \partial_\mu] = 0, \qquad D_{\mathrm{phtn},E} = \mathcal{B}_{\mathrm{cell}}^{\dagger} D_{0,E} \mathcal{B}_{\mathrm{cell}}. \tag{132}$$

The individual release and recapture factors are not separately unique under a reciprocal phase convention; their product is fixed. After analytic continuation a convenient oriented factorization is

$$R_{\mathrm{rel}} = \operatorname{sinc} \frac{K - \Omega}{2}, \qquad R_{\mathrm{rec}} = \operatorname{sinc} \frac{K + \Omega}{2}, \qquad R_{\mathrm{rec}} R_{\mathrm{rel}} = \mathcal{C}_{\mathrm{cell}}. \tag{133}$$

10.6 Calculation domain and minimal continuum completion

The phase-branch dispersion and the continuum response integral have distinct domains. The handoff dispersion identifies the massless branch in a principal phase interval. For the present response model, the analytic characteristic multiplier is extended to continuous boundary Fourier variables and coupled through $\mathcal{A} = \mathcal{B}_{\mathrm{cell}} a$. This is the minimal homogeneous continuum completion used here. A finite Brillouin integration domain would define a different response calculation; it is not silently substituted for the continuum integral.

For a precise inverse, first restrict the Fourier support to

$$\mathcal{S}_{\Lambda,\epsilon,\kappa} = \{k_E : \ \kappa^2 \le k_E^2 \le \Lambda^2, \quad C_E(k_E) \ge \epsilon\}, \qquad \epsilon > 0, \quad \kappa > 0. \tag{134}$$

The scalar aligned multiplier is used in the common vector completion below. On this bounded support, $B_E = C_E^{1/2}$ and B_E^{-1} are bounded multipliers. Source and endpoint factors use the same support as the propagator, so the complete internal-line identity is exact at fixed regulators. This support restriction defines inverse multiplication; it is not a proposed physical phase cutoff or a claim that a sharp-cutoff functional preserves local gauge symmetry. Gauge covariance refers to the untruncated registered action, with a common causal and infrared prescription for the assembled response.

The leading response is defined by assembling the registered exchange first and then removing ϵ, the infrared cutoff, and the ultraviolet cutoff in the finite on-shell Pauli contribution. The resulting convergent parameter integral is evaluated explicitly in Sec. 11. This prescription does not require a bounded inverse on the entire unregulated field space, nor does it establish a full functional-measure equivalence. A different microscopic completion or a retained finite phase cutoff would require its own calculation and could change the response. No such correction is adjusted here to match the measured value.

10.7 From temporal handedness to the transverse vector field

The characteristic theorem above is scalar because the aligned handoff polynomial is the same for both physical temporal-handed branches. The Aether-fabric dynamics nevertheless already contains the data needed to lift that scalar kernel to the two propagating components of the electromagnetic connection.

Let

$$\mathbf{n} \equiv \mathbf{u}_\gamma \tag{135}$$

be the phtn-current direction derived from the six-port state. The dynamically aligned local frame contains an orthonormal transverse pair $\{\mathbf{b}, \mathbf{c}\}$ with $\mathbf{c} = \mathbf{n} \times \mathbf{b}$ Thomson III [2026b]. The two temporal-handed states satisfy

$$H(\omega) h_\eta = e^{-i\eta\omega} h_\eta, \qquad \eta = \pm 1, \tag{136}$$

under a signed link twist ω. Define the circular transverse vectors

$$\boxed{\boldsymbol{\epsilon}_\eta = \frac{1}{\sqrt{2}}(\mathbf{b} + i\eta\mathbf{c}).} \tag{137}$$

A proper rotation by ω about $\mathbf{n}$ sends $\mathbf{b} \mapsto \cos\omega\,\mathbf{b} + \sin\omega\,\mathbf{c}$ and $\mathbf{c} \mapsto -\sin\omega\,\mathbf{b} + \cos\omega\,\mathbf{c}$, so

$$\boxed{\boldsymbol{\epsilon}_\eta \mapsto e^{-i\eta\omega} \boldsymbol{\epsilon}_\eta.} \tag{138}$$

Equations (136) and (138) therefore define an equivariant identification of the two temporal-handed phtn eigenspaces with the two circular transverse polarizations of the aligned spatial frame.

The polarization vectors obey

$$\mathbf{n} \cdot \boldsymbol{\epsilon}_\eta = 0, \qquad \boldsymbol{\epsilon}_\eta^* \cdot \boldsymbol{\epsilon}_{\eta'} = \delta_{\eta\eta'}, \tag{139}$$

and the exact completeness relation

$$\boxed{\sum_{\eta=\pm1} \epsilon_\eta^i \epsilon_\eta^{j*} = \delta^{ij} - n^i n^j \equiv P_T^{ij}.} \tag{140}$$

Thus the two-state phtn fiber supplies exactly two transverse propagating degrees of freedom, not a scalar particle multiplied afterward by a four-vector label.

Section 5 and the prior dual-$U(1)$ construction already establish that the electron couples through a local Abelian connection. The remaining covariant completion is then fixed at quadratic order. The most general parity-even Lorentz-covariant local kernel with at most two derivatives and no mass term is

$$Q^{\mu\nu}(k) = A\, k^2 g^{\mu\nu} + B\, k^\mu k^\nu. \tag{141}$$

Local $U(1)$ gauge invariance requires $Q^{\mu\nu} k_\nu = 0$, hence $A + B = 0$. Canonical normalization fixes the remaining overall coefficient, giving

$$\boxed{Q^{\mu\nu}(k) = -(k^2 g^{\mu\nu} - k^\mu k^\nu),} \tag{142}$$

which is the Fourier kernel of

$$\boxed{S_A = -\frac{1}{4} \int d^4x\, F_{\mu\nu} F^{\mu\nu}.} \tag{143}$$

The physical polarization sum in Eq. (140) is the two-degree-of-freedom content of this gauge action. Adding the standard gauge-fixing term $-(\partial_\mu A^\mu)^2/(2\xi)$ changes only the unphysical longitudinal representation. In Feynman gauge, $\xi = 1$,

$$\boxed{D_{\mu\nu}(k) = \frac{-i g_{\mu\nu}}{k^2 + i0}.} \tag{144}$$

Consequently the four-vector propagator used in the loop is the gauge completion of the two APM phtn helicity modes whose scalar denominator was derived above. The passage from the aligned (X, T) kernel to d^4k therefore uses rotational covariance of the state-derived direction $\mathbf{u}_\gamma$ and the derived transverse polarization frame; it is not an independent promotion of a scalar amplitude to a vector field.

10.8 Registered gauge connection and the complete minimal action

Let a_μ be the underlying APM phtn transport potential and define the registered boundary connection by

$$\boxed{\mathcal{A}_\mu = \mathcal{B}_{\rm cell} a_\mu.} \tag{145}$$

With

$$f_{\mu\nu}[a] = \partial_\mu a_\nu - \partial_\nu a_\mu, \tag{146}$$

translation invariance gives

$$\boxed{F_{\mu\nu}[\mathcal{A}] = \mathcal{B}_{\rm cell} f_{\mu\nu}[a].} \tag{147}$$

The Euclidean phtn action is therefore

$$S_{\rm phtn,E} = \frac{1}{4}\int d^4x\; f_{\mu\nu} C_E f_{\mu\nu} = \frac{1}{4}\int d^4x\; F_{\mu\nu}[\mathcal{A}] F_{\mu\nu}[\mathcal{A}]. \tag{148}$$

Analytic continuation gives the usual metric-dependent sign in Minkowski space. The five-dimensional electron action is

$$S_{e,5} = \int d^4x\, d\tau\; \overline{\Psi}\, \mathscr{D}_5[\mathcal{A}]\Psi, \tag{149}$$

where the covariant derivative contains $D_\mu = \partial_\mu + i q_e \mathcal{A}_\mu$. Equations (108), (148), and (149) complete Eq. (107).

Let

$$J^\mu \equiv q_e\, \overline{\Psi}\gamma^\mu \Psi \tag{150}$$

be the registered matter current. Variation with respect to the underlying phtn field gives

$$\boxed{\mathcal{B}_{\rm cell}^\dagger \left(\partial_\nu F^{\nu\mu} - J^\mu\right) = 0.} \tag{151}$$

Equivalently, in a gauge-fixed transverse scalar channel,

$$\boxed{D_{\rm phtn,E} a = \mathcal{B}_{\rm cell}^\dagger J.} \tag{152}$$

On the physical quotient where $\mathcal{B}_{\rm cell}$ is invertible,

$$\boxed{D_{0,E}\mathcal{A} = J.} \tag{153}$$

Thus the source registration is not an additional assumption: it is the adjoint endpoint factor produced by varying the same action that generates phtn propagation.

10.9 Gauge covariance and the Ward identity

The registered field transforms in the usual way,

$$\Psi \mapsto e^{-iq_e\chi}\Psi, \qquad \mathcal{A}_\mu \mapsto \mathcal{A}_\mu + \partial_\mu \chi. \tag{154}$$

Because $\mathcal{A} = \mathcal{B}_{\rm cell} a$, the underlying phtn potential transforms on the physical quotient as

$$a_\mu \mapsto a_\mu + \mathcal{B}_{\rm cell}^{-1}\partial_\mu \chi. \tag{155}$$

Equation (147) then leaves the phtn kinetic action invariant, while the electron action is invariant by the ordinary covariant-derivative argument. Hence

$$\boxed{\delta_\chi S_{\rm OL}^{\rm min} = 0.} \tag{156}$$

The registered one-particle-irreducible vertex therefore obeys the Ward–Takahashi identity

$$\boxed{q_\mu \Gamma^\mu_{\rm reg}(p', p) = S^{-1}(p') - S^{-1}(p).} \tag{157}$$

Written against the underlying phtn field, one endpoint contributes the scalar registration factor,

$$\Gamma^\mu_{\rm phtn}(p', p; k) = B(k)\, \Gamma^\mu_{\rm reg}(p', p), \tag{158}$$

so the corresponding identity carries the same $B(k)$ factor. A complete internal line removes it through the conjugate endpoint and phtn propagator.

10.10 Minimal tree magnetic response

The microscopic phtn vertex generated by the minimal action is

$$\boxed{V^\mu_{\rm phtn}(k) = -iq_e \gamma^\mu B(k).} \tag{159}$$

The cell factor $B(k)$ is scalar in spinor space. It therefore cannot create an independent $\sigma^{\mu\nu} q_\nu$ structure at tree level. Thus the minimal action gives

$$\boxed{F_1^{(0)}(0) = 1, \qquad F_2^{(0)}(0) = 0, \qquad g_0 = 2.} \tag{160}$$

This is stronger than simply omitting a Pauli coefficient from a boundary Lagrangian: the characteristic-cell reduction itself cannot generate one. The separate gauge-invariant deformation

$$\Delta\mathcal{L}_P = \frac{c_P}{M} \overline{\psi} \sigma^{\mu\nu} F_{\mu\nu} \psi \tag{161}$$

remains mathematically allowed as a nonminimal higher-dimension operator. Accordingly, Eq. (160) proves $c_P^{\rm tree} = 0$ for the minimal Aether-unit action, not that all possible deeper sub-Aether theories must forbid $c_P \neq 0$.

11 Closed Radiative Histories and the One-Loop Pauli Form Factor

11.1 Compact-fiber translation symmetry

The registered boundary connection is independent of the compact temporal-torque coordinate,

$$\boxed{\mathcal{A}_\mu(x, \tau) = \mathcal{A}_\mu(x), \qquad \partial_\tau \mathcal{A}_\mu = 0.} \tag{162}$$

The same is true of $\mathcal{B}_{\rm cell}$, which acts only on boundary space-time coordinates. For normalized compact modes

$$\chi_n(\tau) = \frac{1}{\sqrt{2\pi R_T}} e^{in\tau/R_T}, \tag{163}$$

the phtn vertex satisfies

$$\boxed{\langle n'|V^{\mu}_{\mathrm{phtn}}|n\rangle = -iq_e\gamma^{\mu}B(k)\,\delta_{n'n}.} \tag{164}$$

Equivalently,

$$\boxed{[\widehat{N}_T, V^{\mu}_{\mathrm{phtn}}] = 0, \qquad \Delta n = 0.} \tag{165}$$

Along the connected electron line beginning with a persistent $n = 0$ electron, an ordinary electromagnetic vertex cannot make a $0 \to n \neq 0 \to 0$ excursion unless an explicitly fiber-changing interaction is introduced. An independent closed electron loop may conserve a nonzero n around itself; its allowed sectors are not determined by this external-line argument.

11.2 Exact phtn exchange reduction

In Euclidean Feynman gauge the underlying phtn propagator is

$$\boxed{D^{a,E}_{\mu\nu}(k) = \frac{\delta_{\mu\nu}}{C_E(k)\,k_E^2}.} \tag{166}$$

The two electron–phtn endpoints contribute B_E and $B_E^{\dagger}$. Therefore

$$B_E D^{a,E}_{\mu\nu}(k) B_E^{\dagger} = \frac{B_E B_E^{\dagger}}{C_E(k) k_E^2}\delta_{\mu\nu} \tag{167}$$

$$= \boxed{\frac{\delta_{\mu\nu}}{k_E^2}}. \tag{168}$$

After analytic continuation the same statement is

$$\boxed{R_{\mathrm{rec}}\,\mathcal{D}^{-1}_{\mathrm{phtn}}\,R_{\mathrm{rel}} = \mathcal{D}_0^{-1}.} \tag{169}$$

This equality holds before loop integration on the regulated non-null domain of Sec. 10.6. The continuation is defined through the registered exchange with the same causal prescription. Within this completion, reciprocal poles of the bare operator do not supply additional registered exchange poles; a zero divided by zero is not evaluated separately at an alias.

11.3 Normalized occupied electron weight

The rank-six projector P_- is an admissibility projector, not a six-flavor degeneracy. A physical electron has normalized internal density

$$\rho_e = |\xi_e\rangle\langle\xi_e|, \qquad \mathrm{Tr}_{\mathrm{int}}\,\rho_e = 1, \qquad P_-\rho_e = \rho_e. \tag{170}$$

For the displayed leading vertex graph, every electron segment lies on the open line connected to the normalized external electron. The zero-winding reduction gives its persistent boundary propagator, and evaluation in ξ_e gives $\langle\xi_e|I|\xi_e\rangle = 1$. No independent closed electron loop occurs at this order, so neither a sum over closed-loop compact sectors nor an admissible-rank factor enters this calculation. Higher orders would require an explicit APM rule for those closed histories; $\mathrm{Tr}\,\rho_e = 1$ alone does not supply it.

11.4 One-loop APM phtn vertex correction

Use natural units $\hbar = c = 1$ in this subsection. By the coupling theorem,

$$\alpha_{\text{gauge}} = \alpha_{\text{QMU}} \equiv \alpha_e = \frac{g_{\text{em}}^2}{4\pi}. \tag{171}$$

Before reducing the phtn line, the one-loop vertex correction is

$$\Lambda^{\mu}_{\text{APM}}(p',p) = -ig_{\text{em}}^2 \int \frac{d^4k}{(2\pi)^4}\, \gamma^{\alpha} B_{\text{rec}}(k) S_F(p'-k)\gamma^{\mu} S_F(p-k) \tag{172}$$

$$\times\, \gamma^{\beta} B_{\text{rel}}(k) D^{\text{phtn}}_{\alpha\beta}(k). \tag{173}$$

Equation (169) reduces the complete release–propagation–recapture line exactly, giving

$$\Lambda^{\mu}_{\text{APM}}(p',p) = \Lambda^{\mu}_{\text{reg}}(p',p) \tag{174}$$

with

$$\Lambda^{\mu}_{\text{reg}}(p',p) = -ig_{\text{em}}^2 \int \frac{d^4k}{(2\pi)^4} \frac{\gamma^{\alpha}(\not{p}' - \not{k} + m_e)\gamma^{\mu}(\not{p} - \not{k} + m_e)\gamma_{\alpha}}{[(p'-k)^2 - m_e^2 + i0][(p-k)^2 - m_e^2 + i0][k^2 - \lambda_\gamma^2 + i0]}. \tag{175}$$

The last denominator is therefore not an independently assumed Einstein-photon propagator. It is the registered Green operator of the APM phtn internal line. The fixed APM phtn action scale remains phtn = hc; frequency labels phase/throughput, while the virtual internal line is a Green-function history rather than a persistent $h\nu$ pellet.

Standard on-shell Feynman parametrization isolates the finite Pauli component,

$$F_2^{(1)}(q^2) = \frac{\alpha_{\text{gauge}}}{\pi} m_e^2 \int_0^1 dx\, dy\, dz\, \delta(x+y+z-1) \frac{z(1-z)}{(1-z)^2 m_e^2 - xyq^2 + z\lambda_\gamma^2}. \tag{176}$$

At $q^2 = 0$ the infrared regulator may be removed from the finite Pauli term,

$$F_2^{(1)}(0) = \frac{\alpha_{\text{gauge}}}{\pi} \int_0^1 dz \int_0^{1-z} dy\, \frac{z}{1-z} \tag{177}$$

$$= \frac{\alpha_{\text{gauge}}}{\pi} \int_0^1 z\, dz \tag{178}$$

$$= \boxed{\frac{\alpha_e}{2\pi}}. \tag{179}$$

Thus

$$\boxed{\delta_e^{(1)} = F_2^{(1)}(0) = \frac{\alpha_e}{2\pi}, \qquad |g_e|^{(1)} = 2\left(1 + \frac{\alpha_e}{2\pi}\right).} \tag{180}$$

No measured value of g_e is used to determine the coefficient.

11.5 Scope beyond the calculated order

The registered internal-line identity is sufficient for the leading vertex graph used here. It does not by itself specify the full interacting state space or the weights of independent closed electron histories.

At a finite invertible regulator the linear change $\mathcal{A} = \mathcal{B}_{\rm cell} a$ has a field-independent Jacobian, but a general equivalence theorem would additionally require a specified fermionic measure, internal-sector restrictions, sources, and regulator limits. No all-orders equivalence is claimed in this revision.

The completed prediction is therefore $F_2^{(1)}(0) = \alpha_e/(2\pi)$ within the stated structural model and continuum completion. The next response contribution is open. It may be calculated by extending the APM action and occupied-history rules; it cannot be supplied merely by assuming equality to another theory's higher coefficients.

11.6 Independent force comparison and physical interpretation

The QMU force ledger independently gives

$$\frac{F_E}{F_M} = \frac{\alpha_{\rm QMU}}{2\pi}. \tag{181}$$

The phtn loop gives

$$F_2^{(1)}(0) = \frac{\alpha_{\rm gauge}}{2\pi}. \tag{182}$$

Only the separately derived coupling theorem supplies $\alpha_{\rm QMU} = \alpha_{\rm gauge}$. Therefore

$$\boxed{\frac{F_E}{F_M} = F_2^{(1)}(0) = \frac{\alpha_e}{2\pi}.} \tag{183}$$

The equality is a cross-ledger consistency relation, not the anomaly mechanism.

The internal phtn line also clarifies virtuality in APM language. It is not a persistent free front observed between source and receiver, and it is not an Einstein packet carrying a variable $h\nu$ payload. It is an internal resolvent history of the fixed-action phtn transport field, opened by an LC endpoint and closed by the reciprocal endpoint without independent persistent four-dimensional closure.

12 Quantitative APM Prediction and Empirical Residual

12.1 Prediction in native QMU response coordinates

Combining the calculated vertex with the independently normalized QMU coupling gives

$$\boxed{\delta_e^{(1)} = \frac{e^2}{16\pi^2 e_{e\,\max}^2}, \qquad \frac{|g_e|^{(1)}}{2} = 1 + \frac{e^2}{16\pi^2 e_{e\,\max}^2}.} \tag{184}$$

In the QMU magnetic-response coordinate $\mathcal{E}_\mu = \alpha_e |g_e|/2$,

$$\boxed{\mathcal{E}_\mu^{(1)} = \alpha_e \left(1 + \frac{\alpha_e}{2\pi}\right).} \tag{185}$$

Equivalently, with $\mathrm{magm}_e = e_{e\,\max}^2 \lambda_C^2 F_q$ and $ccf_e = e_{e\,\max}^2/e$, the positive magnetic-moment registration is

$$|\mu_e|^{(1)} ccf_e = \frac{\mathrm{magm}_e}{4\pi} \left(1 + \frac{e^2}{16\pi^2 e_{e\,\max}^2}\right). \tag{186}$$

This supplies the calculated behavior of the occupied structural model in QMU. The baseline, the excess response, and the absolute registration are distinct; the charge conversion is not an additional fitted anomaly factor.

12.2 Independent numerical comparison

We evaluate Eq. (184) using the published recoil inputs

$$\alpha_{\mathrm{Rb}}^{-1} = 137.035999206(11), \tag{187}$$

$$\alpha_{\mathrm{Cs}}^{-1} = 137.035999046(27), \tag{188}$$

from Refs. Morel et al. [2020], Parker et al. [2018]. Neither is obtained by fitting the electron anomaly. They are shown separately rather than averaged. The experimental comparison is the 2023 electron magnetic-moment result Fan et al. [2023],

$$\delta_e^{\mathrm{exp}} = 0.00115965218059(13). \tag{189}$$

The sign convention for the empirical residual is

$$r_e \equiv \delta_e^{(1)} - \delta_e^{\mathrm{exp}}. \tag{190}$$

Table 1: Leading APM response using independent recoil coupling inputs. Uncertainties shown are propagated coupling-input uncertainties, not a theoretical remainder estimate. The residual is prediction minus measurement.

Quantity	Rb recoil	Cs recoil
α^{-1}	137.035999206(11)	137.035999046(27)
$\delta_e^{(1)}$	0.00116140973185	0.00116140973321
$u_\alpha(\delta_e^{(1)})$	9.32×10^{-14}	2.29×10^{-13}
r_e	$+1.75755126 \times 10^{-6}$	$+1.75755262 \times 10^{-6}$
$100 r_e/\delta_e^{\mathrm{exp}}$	+0.15155848%	+0.15155860%
$\mathcal{E}_\mu^{(1)}$	0.00730582777907	0.00730582778761

The rubidium input gives $|g_e|^{(1)} \simeq 2.00232281946370$, compared with the inferred experimental magnitude 2.00231930436118. The model captures the anomaly's sign and leading magnitude; it overshoots its measured value by approximately 0.151558%. The close agreement is reported at that accuracy, not at the experimental precision.

The propagated coupling uncertainty in Table 1 is an input uncertainty only. It is not a theoretical error bar: no bound on omitted response contributions has been derived. The difference between the two recoil inputs is much smaller than the leading residual, so choosing between them cannot remove that residual.

12.3 The remaining difference is an open question

For the rubidium comparison the uncalculated contribution needed to reach the measured value would be $\delta_e^{\mathrm{exp}} - \delta_e^{(1)} \simeq -1.75755126 \times 10^{-6}$. This number is inferred from comparison; it is not

a new APM prediction, coefficient, or interaction. It is not assigned here to higher occupied histories, deeper cell structure, or apparatus response. Each proposed explanation would require an independent derivation and a testable consequence.

The structural model is therefore successful as a leading quantitative approximation under its stated assumptions, while the complete response remains unresolved. This conclusion does not depend on reproducing another theory's mathematical organization. Conversely, simplicity does not eliminate the need to account for the residual if experimental-precision agreement is eventually claimed.

13 Relation to the Earlier Holonomy and Force-Ratio Programs

The earlier QADI electron-$g-2$ paper proposed a forward-time holonomy defect,

$$\delta_e = \Delta_H, \qquad \Delta_H = \frac{1}{2\pi} \oint_{\gamma_+} \delta\omega, \tag{191}$$

with a one-wrap ansatz giving the leading scale $\alpha/(2\pi)$ Thomson III [2026c]. Versions 1.2–1.4 of the present program then emphasized the QMU force ratio and attempted to map that ratio directly into magnetic response. Those approaches identified useful geometry but did not yet derive the Pauli amplitude.

Versions 1.5–1.7 progressively moved the calculation to the correct dynamical object. Version 1.5 used the Pauli form factor but still adopted the ordinary boundary exchange line. Version 1.6 separated α_{QMU} from α_{gauge} and proved their normalization match. Version 1.7 derived compact-mode conservation and normalized one-electron occupancy. Version 1.8 introduced the characteristic-cell internal-line construction. Version 1.9 retained that leading calculation and made its empirical residual explicit. Version 1.10 adds the geometric boundary-matrix reconstruction and a proof delimiting the remaining transport inputs, without importing higher-order coefficients.

The present division of labor is therefore

$$\begin{array}{ll}
\text{QMU charge/action closure} & \longrightarrow \alpha_{\mathrm{QMU}} = \dfrac{k_C e^2}{\hbar c}, \\
U(1)_{es} \text{ source and canonical normalization} & \longrightarrow \alpha_{\mathrm{gauge}} = \alpha_{\mathrm{QMU}}, \\
\text{half-spin boundary factorization} & \longrightarrow g_0 = 2, \\
\text{exact phtn handoff + cell action} & \longrightarrow B_{\mathrm{rec}} G_{\mathrm{phtn}} B_{\mathrm{rel}} = G_{\mathrm{Maxwell}}, \\
\text{closed zero-winding phtn loop} & \longrightarrow F_2^{(1)}(0) = \alpha_{\mathrm{gauge}}/(2\pi), \\
\text{QMU force ledger} & \longrightarrow F_E/F_M = \alpha_{\mathrm{QMU}}/(2\pi).
\end{array} \tag{192}$$

Neither the old holonomy ansatz nor the force ratio is used to evaluate the loop.

14 Epistemic Ledger: Derived, Minimal, and Open

Table 2: Epistemic status of the principal Version 1.10 ingredients.

Status	Statement	Role in this paper
Derived in prior APM/QMU work	$3S+3T$ ontology with fixed-T_E $3S+2T_{\mathrm{dyn}}$ closure; half-angle 4π state; exact one-Aether-unit phtn handoff; scanning-worldsheet and receiver actions; electrostatic $U(1)_{es}$ sector; $A_u = 16\pi^2 k_C$; $A_u e^2_{e\,\max} = hc$; QMU Coulomb law; occupied projector	Supplies the discrete cell, internal topology, charge/action scale, and occupied compatibility structure
Transport closures retained	Selected occupied spin lift; differentiable memoryless unitary boundary evolution; minimal derivative class; reciprocal pair; common speed and native rest loading	Specifies the dynamical choices left open by cell geometry
Constructed here: boundary algebra	Port bivectors and temporal complex orientation give Pauli matrices; parity pairing gives explicit 4×4 gamma matrices and a derived mass shell	Replaces mass-shell-first factorization with a geometric transport reconstruction
Proved limitation	The same geometric data admit H_v with $0 < v \le c$; scalar port projection cannot create a spinorial sign	Identifies the remaining common-speed and occupied-module derivations
Derived coupling match	$\hbar c = 8\pi k_C e^2_{e\,\max}$, $(Q_e^{(es)})^2 = 4\pi e^2$, canonical normalization, and $\alpha_{\mathrm{QMU}} = \alpha_{\mathrm{gauge}}$	Fixes the phtn/electron coupling independently of $g-2$
Derived occupied closure	$S_{\mathrm{seat}} = h\langle \Xi, Q_- \Xi\rangle$, zero-winding reduction, ρ_e with $\mathrm{Tr}\,\rho_e = 1$, and $\Delta n = 0$	Fixes the external occupied-line weight at the calculated order; closed-history weights remain open
Derived here: local boundary wave operator	Exact aligned $\Omega^2 = K^2$ plus locality, reciprocal evenness in K and Ω, gaplessness, and minimal second-order dynamics give $\mathcal{D}_0 = \partial_T^2 - \partial_X^2 = -\partial_u \partial_v$	Removes the massless continuum operator as an independent photon premise
Derived here: transverse vector lift	$h_\eta \leftrightarrow \boldsymbol{\epsilon}_\eta = (\mathbf{b} + i\eta\mathbf{c})/\sqrt{2}$, $\sum_\eta \epsilon^i_\eta \epsilon^{j*}_\eta = \delta^{ij} - n^i n^j$, and the minimal Lorentz-covariant, parity-even $U(1)$ completion gives the Maxwell kernel	Derives the two physical vector polarizations and the covariant gauge completion of the scalar phtn denominator
Derived here: characteristic registration	$\mathcal{D}_{\mathrm{phtn}} = \mathcal{A}_{\mathrm{cell}} \mathcal{D}_0$ with $\mathcal{C}_{\mathrm{cell}} = \mathrm{sinc}[(K-\Omega)/2]\,\mathrm{sinc}[(K+\Omega)/2]$ and diamond kernel $\frac{1}{2}\mathbf{1}_{\lvert X\rvert+\lvert T\rvert\le 1}$	Makes the cell profile a variational consequence rather than an appended filter
Derived here: square-root phtn map	In Euclidean signature $C_E \ge 0$; on the regulated non-null support, $\mathcal{B}_{\mathrm{cell}} = C_E^{1/2}$, $\mathcal{A} = \mathcal{B}_{\mathrm{cell}} a$, and $F[\mathcal{A}] = \mathcal{B}_{\mathrm{cell}} f[a]$	Identifies the registered boundary connection as the physical image of the underlying phtn potential
Derived here: gauge closure	$\delta_\chi S^{\min}_{\mathrm{OL}} = 0$ and $q_\mu \Gamma^\mu = S^{-1}(p') - S^{-1}(p)$	Preserves charge normalization and the Ward identity
Derived here: phtn exchange reduction	$B_{\mathrm{rec}} G_{\mathrm{phtn}} B_{\mathrm{rel}} = G_{\mathrm{Maxwell}}$ before loop integration	Replaces the imported boundary photon line with the registered APM phtn line
Derived here: minimal tree response	Scalar cell registration cannot generate a tree Pauli tensor, so $F_2^{(0)}(0) = 0$ and $g_0 = 2$	Closes the minimal tree magnetic response; a separately added dimension-five operator remains nonminimal
Calculated here	$F_2^{(1)}(0) = \alpha_e/(2\pi)$ from the phtn loop after exact internal-line reduction	Produces the leading electron anomaly without using the QMU force ratio
Model completion retained	Analytic continuum registration with a common non-null regulator; continuum limit taken for the assembled leading response	Defines the momentum domain of the calculated prediction
Empirical comparison	Independent recoil coupling gives a leading residual of approximately $+1.75755 \times 10^{-6}$	Establishes the achieved accuracy; does not calculate the missing contribution

Status	Statement	Role in this paper
Open beyond leading order	Closed occupied-history weights and additional interaction response	No all-orders numerical prediction or error bound is claimed
Independent QMU calculation	$F_E/F_M = \alpha_{\mathrm{QMU}}/(2\pi)$	Becomes a cross-ledger equality only after the separate coupling theorem
Open below Aether-unit resolution	Derive the primitive coherent Aether Unit, the selected spinorial occupied map, memoryless minimal transport and common-speed closure, detailed ξ_e, and possible nonminimal Pauli or nontrivial dual-$U(1)$ operators from deeper mechanics	Defines foundational questions in addition to the open empirical residual

15 Empirical Tests and the Open Response Boundary

The minimal registered exchange has no extra cell factor in the displayed leading Pauli integral. This is a statement about the assembled exchange within the specified continuum completion, not a theorem that all APM corrections vanish. The measured residual in Sec. 12 remains part of the scientific result.

The empirical remainder is approximately $-0.326(\alpha_e/\pi)^2$, providing a quantitative sign and scale against which an independently derived additional APM response can be tested; this numerical comparison does not identify its mechanism or perturbative order.

A future extension should calculate an additional response from fixed APM rules before comparing it with the residual. Examples requiring investigation include additional occupied histories, a microscopically generated nonminimal magnetic coupling, nonuniform registration, or an independently derived electron–apparatus interaction. Their coefficients must not be selected from the target anomaly. A finite phase-domain model must likewise calculate its cutoff effect rather than choose a boundary to reproduce the data.

The most direct experimental route is to predict spin and motional frequency responses in a specified trap. An apparatus-dependent explanation would need a definite dependence on magnetic field, cavity dimensions, or another controlled setting. A universal correction would need consistency across such settings. The present calculation contains no evidence that the published measurement was adjusted toward a theoretical expectation, and no apparatus contribution is used to cancel its residual.

There is no controlled remainder estimate yet, so the leading approximation alone cannot support exclusion limits at the experimental uncertainty. It does provide a definite leading formula, a transparent set of inputs, and a quantitative target for the next APM calculation.

16 Discussion

16.1 What has changed conceptually

The structural contribution is the characteristic-cell construction underlying the calculated leading response. It is the identification of the continuum electromagnetic exchange line as the registered Green operator of the APM phtn. The phtn remains a fixed-action transport object in APM ontology;

the familiar massless propagator emerges only after the complete LC endpoint–phtn–endpoint history is assembled.

16.2 Why the characteristic cell is dynamical

The cell kernel is fixed twice by the same structure. Its bulk Fourier multiplier is forced by $\mathcal{D}_{\mathrm{phtn}} = \mathcal{A}_{\mathrm{cell}}\mathcal{D}_0$, and the action variation gives the conjugate endpoint factor that registers the matter current. Within the stated completion, reciprocal aliases are zeros of registration. Their inverse treatment is controlled by the common non-null prescription of Sec. 10.6; a different finite phase-domain model is not excluded.

The Stage-11D loxodrome and the characteristic diamond have different jobs. The loxodrome encodes occupied channel topology and scan order. The characteristic diamond is the causal support of one inter-Unit handoff in the aligned longitudinal-time plane. Their geometries should not be conflated.

16.3 Why the Ward identity matters

A momentum-dependent endpoint form factor can easily destroy gauge consistency if it is introduced by hand. Here the factor arises through the field map $\mathcal{A} = \mathcal{B}_{\mathrm{cell}}a$, with $\mathcal{B}_{\mathrm{cell}}$ scalar and translation invariant. The complete action therefore remains locally $U(1)$ covariant and the registered vertex obeys the ordinary Ward–Takahashi identity. This is the main reason the phtn reduction can be used inside radiative graphs without changing charge renormalization.

16.4 Tree Pauli term and deeper dynamics

The minimal action produces only the vector current multiplied by a scalar registration factor, so no tree Pauli tensor is generated. This is a real derivation of $F_2^{(0)}(0) = 0$ within the minimal Aether-unit theory. It does not prove that a deeper theory cannot produce

$$\frac{c_P}{M}\bar{\psi}\sigma^{\mu\nu}F_{\mu\nu}\psi.$$

Such a term would represent new microscopic information and must be calculated or bounded independently.

16.5 What the leading calculation establishes

The boundary matrices are constructed from the port spin frame and reciprocal propagation pair, and their mass shell follows within the stated transport closure. The local characteristic operator follows within the minimal derivative class; the transverse lift uses the two temporal-handed phtn states and a minimal covariant completion. The registration and conjugate endpoint factors then yield the finite leading response. The underdetermination result in Sec. 5.7 shows why the remaining transport choices cannot be claimed as consequences of geometry alone.

Its economy is that no anomaly-specific coefficient is adjusted: the measured charge coordinate and the structural interaction determine the leading excess. Its limitation is that the paper does not

determine the full response or a controlled remainder. The residual remains an open result rather than being removed through a calibration or an asserted all-orders equivalence.

17 Conclusions

The occupied-Ligamen model gives a simple leading electron magnetic response from APM structure and QMU behavior. QMU charge/action closure and source normalization give

$$\alpha_e = \frac{e^2}{8\pi e^2_{e\,\max}} = \frac{g^2_{\mathrm{em}}}{4\pi}. \tag{193}$$

The port-spin and reciprocal-pair construction supplies explicit boundary matrices and the mass shell under the stated transport closure. Its fixed-polarity, zero-winding, minimally coupled sector gives $g_0 = 2$. The characteristic-cell factorization and registered endpoints give the massless internal exchange within the stated continuum completion. The calculated Pauli response is

$$\boxed{\delta_e^{(1)} = \frac{\alpha_e}{2\pi} = \frac{e^2}{16\pi^2 e^2_{e\,\max}}, \qquad \mathcal{E}_\mu^{(1)} = \alpha_e\left(1 + \frac{\alpha_e}{2\pi}\right).} \tag{194}$$

The equal QMU force ratio is a consistency relation, not a substitute for this response calculation.

With the independent rubidium recoil coupling, the leading anomaly is 0.00116140973185. The measured comparison is 0.00115965218059(13), leaving a predicted-minus-measured residual of $+1.75755126 \times 10^{-6}$, approximately 0.151558% of the measured anomaly. The cesium recoil input leaves essentially the same discrepancy. Input uncertainties are much smaller than this residual; theoretical uncertainty beyond the calculated order is not bounded here.

The paper therefore establishes a viable leading quantitative approximation within its assumptions, not experimental-precision reproduction of the electron anomaly or validation of the entire APM. No higher-order coefficients, apparatus adjustments, or fitted anomaly terms are used to close the difference. Its origin remains open. The next scientific step is an independently specified APM calculation of further response or a discriminating experimental dependence.

A Electrostatic Charge, Magnetic Charge, and the Charge Conversion Factor

A.1 Why a conversion factor is required

QMU and SI do not use the same primitive charge registration for every electromagnetic quantity. In the electron QMU system the Charge Conversion Factor is

$$\boxed{ccf_e = \frac{e^2_{e\,\max}}{e} = \frac{e}{8\pi\alpha_e}, \qquad \alpha_e = \alpha_{\mathrm{QMU}} = \alpha_{\mathrm{gauge}}.} \tag{195}$$

The CCF is not an adjustable constant. It is the bridge between singular SI charge registration and the distributed magnetic square-charge registration used by QMU Thomson III [2025b].

For a numerator charge quantity, conversion from QMU to the corresponding SI registration introduces ccf_e; denominator charge quantities transform inversely. Squared dynamic quantities require the corresponding squared conversion. QMU quantities whose definitions already absorb the charge registration must be treated according to their specific ledger identities rather than by indiscriminate dimensional substitution.

A.2 Magnetic moment example

The QMU magnetic-moment standard is $\mathrm{magm}_e = e^2_{e\,\max}\lambda_C^2 F_q$, whereas μ_e is the signed experimental electron magnetic moment and $|\mu_e|$ is its magnitude. Their bridge is a conversion identity. It is not used in the main derivation of $g_0 = 2$; rather, it provides a downstream QMU registration of the tree-level value already obtained from the minimally coupled boundary spinor. The bridge is

$$\boxed{|\mu_e|\, ccf_e = \frac{|g_e|\mathrm{magm}_e}{8\pi} = \frac{\mathcal{E}_\mu\, \mathrm{magm}_e}{4\pi\alpha_e}.} \tag{196}$$

For the Bohr baseline,

$$\boxed{\mu_B\, ccf_e = \frac{\mathrm{magm}_e}{4\pi} = \frac{\alpha_e\, \mathrm{magm}_e}{4\pi\alpha_e},} \tag{197}$$

which corresponds to $\mathcal{E}_\mu^{(0)} = \alpha_e$. Hence

$$\frac{|\mu_e| - \mu_B}{\mu_B} = \frac{|g_e| - 2}{2} = \delta_e, \tag{198}$$

with the CCF cancelling in the same-species ratio. This illustrates why the CCF is essential for absolute SI–QMU conversion but disappears from properly formed dimensionless response ratios Thomson III [2026d].

A.3 Two-charge summary

Quantity	APM/QMU role
e and e^2	electrostatic charge registration associated with the static electrostatic sector
$e^2_{e\,\max}$	distributed electron magnetic square-charge generated from LC angular momentum through Aether conductance
$ccf_e = e^2_{e\,\max}/e$	SI–QMU charge-registration bridge
F_E	electrostatic force channel at the electron quantum scale
F_M	magnetic/Aether force channel at the same scale; equals one native electron `forc`
magm_e	QMU magnetic-moment measurement standard; not the measured particle moment
μ_e	experimentally measured electron magnetic moment

The SI bridge constants below are CODATA 2022 recommended values Mohr et al. [2025]. The independent recoil coupling inputs used for the empirical test are listed separately in Sec. 12; the CODATA coupling is retained for reference only.

B Constants Used in SI Comparisons

Numerical constants used for SI comparison are taken from the latest CODATA recommended values [Mohr et al., 2025]. All derivations in the main text remain QMU-first.

Table 3: Physical constants used for SI comparison. Values are taken from the latest CODATA recommended constants [Mohr et al., 2025]. The QMU role column identifies how each constant is used in the ledger, bridge, or closure structure of the paper.

Symbol	Description	Value	Unit	QMU role
c	speed of light	299792458	$\mathrm{m\,s^{-1}}$	SI bridge for $F_q\lambda_C$
m_e	electron mass	$9.1093837139 \times 10^{-31}$	kg	base-mass bridge for m_e
λ_C	electron Compton wavelength	$2.42631023538 \times 10^{-12}$	m	base-length bridge for λ_C
α	fine-structure constant	$7.2973525643 \times 10^{-3}$	dimensionless	boundary electromagnetic coupling; QMU charge-ledger bridge
α^{-1}	inverse fine-structure constant	137.035999177	dimensionless	inverse coupling bridge

C Standard-Physics Bridge and Numerical Provenance

The main prediction is dimensionless and QMU-first. Canonical field coordinates and natural units are used only to evaluate its response integral. SI mass, length, and charge values in the constants table supply conversion context; the numerical prediction requires an empirical dimensionless coupling, supplied independently by atom recoil in Sec. 12.

The published electron frequency analysis and the inferred anomaly are experimental comparisons, not inputs to the coefficient $1/(2\pi)$. No QED higher-order value is used in the APM numerical result. The measured residual has not been corrected for an APM apparatus effect, because no such effect is calculated here.

The supplied `reproduce.py` uses only the Python standard library. It calculates both recoil-based predictions, input uncertainty propagation, signed and normalized residuals, relative errors, and the QMU response coordinate. It checks the port quaternion algebra, explicit gamma matrices, reciprocal generator, frame covariance, unitary evolution, native QMU dispersion, and slower same-geometry counterfamily, together with the cell identity, normalized diamond kernel, and leading parameter integral. The checks reproduce algebra and arithmetic; they do not establish the underlying physical assumptions. Generated JSON, CSV, and the numerical table accompany the source.

D Compact Derivation Summary

For reference, the Version 1.10 leading-response chain can be compressed to

$$\alpha_{\mathrm{QMU}} \equiv \frac{e^2}{8\pi e_{e\,\max}^2}, \tag{199}$$

$$A_u e_{e\,\max}^2 = hc, \qquad A_u = 16\pi^2 k_C, \tag{200}$$

$$\hbar c = 8\pi k_C e_{e\,\max}^2, \tag{201}$$

$$\alpha_{\mathrm{QMU}} = \frac{k_C e^2}{\hbar c}, \tag{202}$$

$$(Q_e^{(es)})^2 = 4\pi e^2, \tag{203}$$

$$g_{\mathrm{em}} = |Q_e^{(es)}| \sqrt{\frac{k_C}{\hbar c}}, \tag{204}$$

$$\alpha_{\mathrm{gauge}} \equiv \frac{g_{\mathrm{em}}^2}{4\pi} = \alpha_{\mathrm{QMU}} \equiv \alpha_e, \tag{205}$$

$$\zeta_h(\Phi) = e^{ih\Phi/2}, \qquad \zeta_h(\Phi + 4\pi) = \zeta_h(\Phi), \tag{206}$$

$$\mathsf{a}_i = \varrho_3 \otimes \sigma_i, \quad \mathsf{b} = \varrho_1 \otimes I_2, \tag{207}$$

$$\gamma^0 = \mathsf{b}, \quad \gamma^i = \mathsf{b}\mathsf{a}_i, \tag{208}$$

$$\{\gamma^\mu, \gamma^\nu\} = 2\eta^{\mu\nu} I, \tag{209}$$

$$D_\mu = \partial_\mu + i q_e \mathcal{A}_\mu, \qquad |q_e| = g_{\mathrm{em}}, \tag{210}$$

$$\Pi_{\mathrm{cl}} P_- \mathscr{D}_5^{-1} P_- \Pi_{\mathrm{cl}} = S_F^{(4)} \otimes P_-, \tag{211}$$

$$\rho_e = |\xi_e\rangle\langle\xi_e|, \qquad \mathrm{Tr}_{\mathrm{int}}\, \rho_e = 1, \tag{212}$$

$$X = x_\parallel/\lambda_C, \quad T = t/t_q, \quad u = (X+T)/2, \quad v = (X-T)/2, \tag{213}$$

$$\mathcal{D}_{\mathrm{phtn}} = -\Delta_u \Delta_v, \qquad \mathcal{D}_0 = -\partial_u \partial_v, \tag{214}$$

$$\mathcal{D}_{\mathrm{phtn}} = \mathcal{A}_{\mathrm{cell}} \mathcal{D}_0, \tag{215}$$

$$\mathcal{C}_{\mathrm{cell}}(\Omega, K) = \mathrm{sinc}\, \frac{K-\Omega}{2}\, \mathrm{sinc}\, \frac{K+\Omega}{2}, \tag{216}$$

$$C_E = \frac{2(\cosh \Omega_E - \cos K)}{K^2 + \Omega_E^2}, \tag{217}$$

$$\mathcal{B}_{\mathrm{cell}} = C_E^{1/2}, \qquad \mathcal{A} = \mathcal{B}_{\mathrm{cell}} a, \tag{218}$$

$$F[\mathcal{A}] = \mathcal{B}_{\mathrm{cell}} f[a], \tag{219}$$

$$\mathcal{B}_{\mathrm{cell}}^\dagger (\partial_\nu F^{\nu\mu} - J^\mu) = 0, \tag{220}$$

$$\delta_\chi S_{\mathrm{OL}}^{\min} = 0, \tag{221}$$

$$q_\mu \Gamma_{\mathrm{reg}}^\mu = S^{-1}(p') - S^{-1}(p), \tag{222}$$

$$V_{\mathrm{phtn}}^\mu(k) = -i q_e \gamma^\mu B(k), \tag{223}$$

$$F_2^{(0)}(0) = 0, \qquad g_0 = 2, \tag{224}$$

$$[\widehat{N}_T, V_{\mathrm{phtn}}^\mu] = 0, \qquad \Delta n = 0, \tag{225}$$

$$B_{\mathrm{rec}} \mathcal{D}_{\mathrm{phtn}}^{-1} B_{\mathrm{rel}} = \mathcal{D}_0^{-1}, \tag{226}$$

$$Z_{\mathrm{APM}}^{\min} \propto Z_{\mathrm{bdy}}, \tag{227}$$

$$\mathcal{M}^{(N)}_{\mathrm{APM,phys}} = \mathcal{M}^{(N)}_{\mathrm{bdy}}, \tag{228}$$

$$F_2^{(1)}(0) = \frac{\alpha_e}{\pi}\int_0^1 z\,dz = \frac{\alpha_e}{2\pi}, \tag{229}$$

$$|g_e|^{(1)} = 2\left(1 + \frac{\alpha_e}{2\pi}\right), \tag{230}$$

$$\frac{F_E}{F_M} = \frac{\alpha_{\mathrm{QMU}}}{2\pi} = F_2^{(1)}(0), \tag{231}$$

$$\delta_e = F_2(0). \tag{232}$$

E Notation for the Updated Chronogeometric Model

Symbol	Meaning
Π_T	forward/backward temporal phase
Π_S	left/right temporal-torque phase
J_T	canonical complex structure of the temporal plane
L_i, σ_i	port-plane quaternion generators and their Pauli representation
ϱ_i	Pauli matrices on the reciprocal boundary propagation pair
a_i, b	explicit boundary transport matrices, $\varrho_3 \otimes \sigma_i$ and $\varrho_1 \otimes I_2$
E_q	native electron rest loading, $m_e\mathrm{temp} = hF_q$
h_η	temporal-handed eigenstate, $\eta = \pm 1$
τ	compact temporal-torque coordinate
n	compact temporal-fiber Fourier mode number
P_s	occupied parity–handedness projector
P_-	rank-six electron admissibility projector in the current species convention
ρ_e	normalized one-electron internal occupancy density, $\lvert\xi_e\rangle\langle\xi_e\rvert$ with $\mathrm{Tr}_{\mathrm{int}}\,\rho_e = 1$
$\widehat{N}_T$	compact temporal-mode generator, $-iR_T\partial_\tau$
X, T	dimensionless aligned longitudinal and exposed-time coordinates, $x_\parallel/\lambda_C$ and t/t_q
u, v	reciprocal characteristic coordinates, $(X+T)/2$ and $(X-T)/2$
$\mathcal{A}_{\mathrm{cell}}$	derived one-handoff characteristic-cell registration operator
$\mathcal{C}_{\mathrm{cell}}$	Fourier multiplier of $\mathcal{A}_{\mathrm{cell}}$, the product of two sinc factors
$\mathcal{B}_{\mathrm{cell}}$	positive Euclidean square-root registration operator, $C_E^{1/2}$, used to map the underlying phtn potential to the registered connection
a_μ	underlying APM phtn transport potential before characteristic-cell registration
$\mathcal{A}_\mu$	registered boundary gauge connection, $\mathcal{A}_\mu = \mathcal{B}_{\mathrm{cell}} a_\mu$
$\mathcal{D}_{\mathrm{phtn}}$	exact aligned inverse phtn handoff operator, $-\Delta_u\Delta_v$
$\mathcal{H}_{\mathrm{phys}}$	formal quotient by cell-unresolved alias modes; inverse registration is defined on the regulated non-null support in Sec. 10.6
Π_{cl}	zero-net-winding boundary projector
$\mathscr{D}_5$	minimal five-dimensional electron kinetic operator
G_5	five-dimensional propagator
S_F	ordinary four-dimensional Dirac/Feynman propagator
t_q	one exposed QMU quantum moment, $1/F_q$
e	QMU electrostatic charge magnitude appearing in the Coulomb ledger
$Q_e^{(es)}$	signed source coefficient in the $1/(4k_C)$ electrostatic gauge normalization
q_e	signed canonical boundary charge, $q_e = Q_e^{(es)}\sqrt{k_C/(\hbar c)}$, with $\lvert q_e\rvert = g_{\mathrm{em}}$
g_{em}	positive canonically normalized dimensionless boundary gauge coupling
α_{QMU}	QMU charge coordinate, $e^2/(8\pi e^2_{e\,\max})$
α_{gauge}	canonical gauge coordinate, $g^2_{\mathrm{em}}/(4\pi)$; proved equal to α_{QMU} in Sec. 4
$\mathcal{E}_\mu$	transposed QMU magnetic-response coordinate, $\alpha_e\lvert g_e\rvert/2$; downstream registration only
$F_2(0)$	zero-momentum Pauli form factor, equal to δ_e

Acknowledgments

The Quantum AetherDynamics Institute is a U.S. 501(c)(3) public charity and independent nonprofit research organization developing the Aether Physics Model (APM) and Quantum Measurement Units (QMU) Thomson III [2025a]. Publications and data are archived with DOIs in the AetherPhysics Zenodo community: zenodo.org/communities/aetherphysics.

References

P. A. M. Dirac. The quantum theory of the electron. *Proceedings of the Royal Society of London. Series A*, 117(778):610–624, 1928. doi: 10.1098/rspa.1928.0023.

X. Fan, T. G. Myers, B. A. D. Sukra, and G. Gabrielse. Measurement of the electron magnetic moment. *Physical Review Letters*, 130:071801, 2023. doi: 10.1103/PhysRevLett.130.071801.

Peter J. Mohr, David B. Newell, Barry N. Taylor, and Eite Tiesinga. Codata recommended values of the fundamental physical constants: 2022. *Reviews of Modern Physics*, 97:025002, 2025. doi: 10.1103/RevModPhys.97.025002.

Léo Morel, Zhibin Yao, Pierre Cladé, and Saïda Guellati-Khélifa. Determination of the fine-structure constant with an accuracy of 81 parts per trillion. *Nature*, 588:61–65, 2020. doi: 10.1038/s41586-020-2964-7.

Richard H. Parker, Chenghui Yu, Weicheng Zhong, Brian Estey, and Holger Müller. Measurement of the fine-structure constant as a test of the Standard Model. *Science*, 360(6385):191–195, 2018. doi: 10.1126/science.aap7706.

Julian Schwinger. On quantum-electrodynamics and the magnetic moment of the electron. *Physical Review*, 73:416–417, 1948. doi: 10.1103/PhysRev.73.416.

David W. Thomson III. Quantum aetherdynamics institute (qadi): Community doi overview and citation guide. Zenodo, 2025a. URL https://doi.org/10.5281/zenodo.17479314.

David W. Thomson III. The charge conversion factor in the aether physics model: From singular to distributed charge, with rules, exceptions, and benchmarks, 2025b. URL https://doi.org/10.5281/zenodo.17451188.

David W. Thomson III. Dual-$u(1)$ aether electrodynamics with topological mixing in qmu, 2025c. URL https://doi.org/10.5281/zenodo.17353425.

David W. Thomson III. Topological uniqueness of $a_u/k_c = 16\pi^2$ in the aether physics model (qmu), 2025d. URL https://doi.org/10.5281/zenodo.17336682.

David W. Thomson III. The chronogeometry of the aether unit: Orthogonal temporal dimensions, $16\pi^2$ state space, and ledger-one deformation closure, 2026a. URL https://doi.org/10.5281/zenodo.21538113.

David W. Thomson III. The dynamical geometry of the aether fabric: Frame-transported six-port propagation, two-state temporal closure, and exact recovery of the photon speed, 2026b. URL https://doi.org/10.5281/zenodo.21607739.

David W. Thomson III. Electron $g - 2$ closure from aether-unit holonomy in qmu, 2026c. URL https://doi.org/10.5281/zenodo.18707059.

David W. Thomson III. QMU registration of gyroscopic coupling in a nonspinning ferromagnet: Public-trace reproduction, a composition envelope, and a material-participation constraint, 2026d. URL https://doi.org/10.5281/zenodo.21862332.

David W. Thomson III. The five-dimensional one-spin phtn of the aether fabric: Paired half-spin loxodromes, quadratic cardioid projection, and species-scale transport, 2026e. URL https://doi.org/10.5281/zenodo.21655869.

David W. Thomson III. The chirality-matched receiver of the aether fabric: Invariant boundary action, one-moment spectral selection, and the triadic capture matrix, 2026f. URL https://doi.org/10.5281/zenodo.21631888.

David W. Thomson III. The scanning mass string and occupied-channel closure of the aether fabric: Time-integrated exposure, species chirality, and the rank-six compatibility gate, 2026g. URL https://doi.org/10.5281/zenodo.21630943.

David W. Thomson III. Unified force structure in quantum measurement units: Distributed magnetic charge, common aether closure, and the electron electrostatic–magnetic force ratio, 2026h. URL https://doi.org/10.5281/zenodo.20585418.